ACES Asian Chemical Editorial Society

doi.org/10.1002/cnma.202100235

CHEMNANOMAT
Minireview

Materials Development in Hybrid Zinc-Ion Capacitors

Ajay Dattu Jagadale,*[a] Ravichandran Chitra Rohit,[a] Surendra Krushna Shinde,[b] and Dae-Young Kim[b]

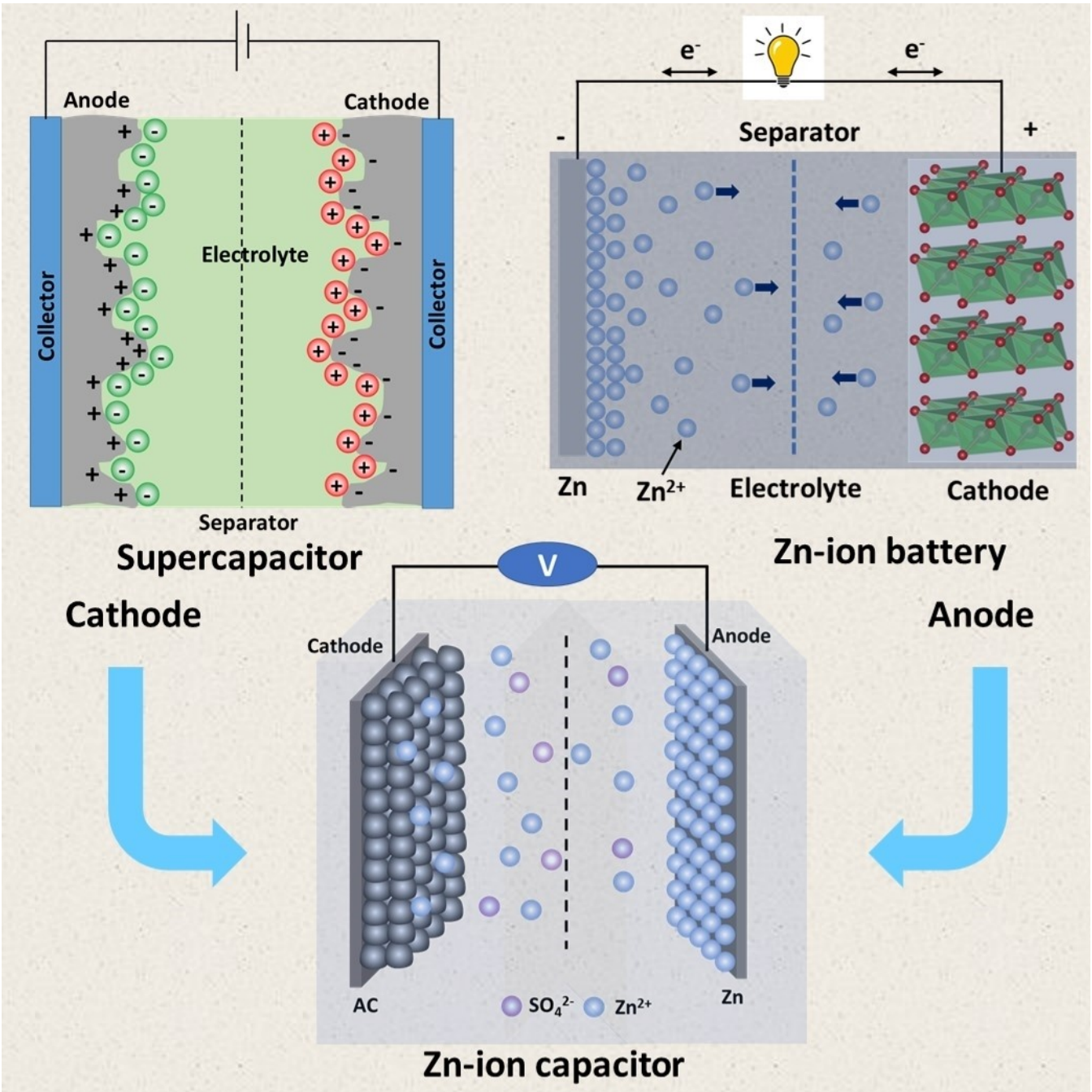

Abstract: High-performance energy storage devices have an exceptional role in modern applications such as green transportation, consumer electronics and electrical systems. Recently, the hybrid supercapacitor has gained great interest among researchers that adopt a combination of capacitive and battery-type electrodes to increase the energy density without sacrificing the power performance. Different types of hybrid energy storage devices have been reported recently including lithium-ion capacitor (LIC), sodium-ion capacitor (NIC) and potassium-ion capacitor (KIC). However, these devices are based on alkali metals such as Li, Na and K which are extremely reactive and consistently used with flammable organic electrolytes that intensify serious safety issues. Hybrid devices based on multivalent ions including Mg^{2+}, Ca^{2+}, Al^{3+} and Zn^{2+} have achieved considerable attraction due to their rapid charge transfer kinetics and high capacity as well as energy density. Herein, we reviewed the recent developments in the anode and cathode materials of Zinc ion hybrid capacitors (ZICs). The design, construction and working of supercapacitor (SC), Zinc ion battery (ZIB) and ZIC have been discussed along with their charge storage mechanism. Finally, based on the published work, our views on future developmental opportunities have been discussed.

1. Introduction

The drastic utilization and the limited availability of fossil fuels are some of the major reasons for the current energy and environmental crisis.[1] These issues can be resolved by adopting green and renewable energy sources including wind, solar and tidal energies.[2,3] However, since these are intermittent sources, the development of high-performance energy storage devices has become one of the important research directions.[4,5] Due to high performance and reliability, supercapacitors (SCs) and batteries have attracted tremendous attention and have been extensively researched over the last two decades. An SC has been considered as a promising energy storage device owing to its exceptional role in the field of green transportation, consumer electronics and electrical systems.[6–10] The SC is the type of electrochemical energy storage device which offers a very high power density, long life, fast charging/discharging rate and good safety.[11–13] The charge storage mechanism of the SC involves an electric double-layer capacitor (EDLC) and pseudocapacitor. The EDLC stores charge by physical adsorption/desorption of ions on the electrode surface, while the pseudocapacitor involves rapid redox reactions at/near the surface of the electrode.[4,14] SCs are mainly suffered from their poor energy density and fast self-discharge behavior. Moreover, batteries are high energy density electrochemical energy storage devices in which charge is stored via faradaic redox reactions.[15–18] The major hurdle in batteries is their poor power performance and limited cycle life. Apart from SCs and batteries, the concept of a hybrid SC has gained great attention that uses combination of capacitive and battery-type electrodes to increase the energy density without sacrificing the power performance.[19–21] The hybrid SC has an imperative role in industrial power supplies, public transport vehicles, smart-grids, and consumer electronics.[22] Different types of hybrid energy storage devices have been reported recently including lithium-ion capacitor (LIC),[23–26] sodium-ion capacitor (NIC)[27–30] and potassium-ion capacitor (KIC).[31–34] However, these devices are based on alkali metals such as Li, Na and K which are extremely reactive and always used with flammable organic electrolytes, intensifying the serious safety issues. Besides, a scarcity of lithium resources as well as its high demand in the automobile and electronics industries have made it valuable and expensive. Alternately, hybrid devices based on multivalent ions including Mg^{2+}, Ca^{2+}, Al^{3+} and Zn^{2+} have gained great attraction due to their fast charge transfer kinetics, high capacity and energy density. In addition, most of these multivalent cations are earth-abundant and offer a multi-electron transfer-driven storage mechanism.[35]

Recently, different multivalent ions-based hybrid capacitors have been reported including, magnesium-ion,[36–39] calcium-ion,[40] aluminum-ion[41–43] and zinc-ion capacitors.[44–46] Among these, zinc-ion capacitors (ZICs) have received great importance owing to a high gravimetric capacity (823 $mAh \cdot g^{-1}$) and low redox potential of −0.76 V vs. the standard hydrogen electrode of Zn metal. Also, ZICs combine merits of Zn-ion batteries including low cost and environmental friendliness and advantages of SCs such as rapid charge-discharge, high power and long cycle life. Interestingly, the performance of ZIC is highly comparable with other alkali metal ion-based hybrid capacitors (Table 1).[10,47,48] The concept of ZIC was proposed by Wang et al.,[49] they combined Zn metal anode, carbon nanotubes cathode and $ZnSO_4$ aqueous electrolyte. Although the performance of this ZIC was inferior, that work emerged as a stimulus

[a] *Dr. A. D. Jagadale, R. C. Rohit*
Centre for Energy Storage and Conversion, School of Electrical and Electronics Engineering
SASTRA Deemed University
Thanjavur 613401, Tamil Nadu (India)
E-mail: jagadaleajay99@gmail.com
[b] *Dr. S. K. Shinde, Prof. D.-Y. Kim*
Department of Biological and Environmental Science, College of Life Science and Biotechnology
Dongguk University
32 Dongguk-ro, Biomedical Campus, Ilsandong-gu, Siksa-dong, 10326, Goyang-si, Gyeonggi-do (South Korea)

Table 1. Comparison of energy storage performance of ZIC and other alkali metal ion capacitors.

Device	Energy density [$Wh.kg^{-1}$]	Power density [$W.kg^{-1}$]	Cycle life
LIC	19–262	300–156000	<75000
NIC	6–320	12–20800	<10000
KIC	12–187	599–25600	<55000
ZIC	34–605	36–23500	<20000

for subsequent developments in the field. Much work has been focused on preparing novel high-performance anode, cathode and electrolyte materials. Recently, many review articles have been presented on Zn-ion batteries,[50–55] however, only a few review articles have been published on ZICs with a lack of discussion on the development of materials, storage mechanisms involved, comprehensive literature review of anode, cathode and electrolyte materials.[35,56–60]

Herein, we focus on reviewing the recent progress of anode, cathode and electrolyte of Zinc ion hybrid capacitors. The design, construction and working of SCs, ZIBs and ZICs have been discussed along with their charge storage mechanism. The electrode material engineering, device configuration, energy storage mechanism and electrochemical performance of ZIC were elucidated. Finally, based on the published work, our views on future developmental opportunities have been provided.

2. SCs, ZIB and ZIC

SCs are mainly formed of activated porous carbon electrodes and the aqueous/non-aqueous electrolyte. The charge storage is based on the reversible accumulation of ions on the electrode surface. As shown in Figure 1, when the electrode is polarized, the Helmholtz layer is formed, leading to a separation of charge at the electrode/electrolyte interface. Besides, to maintain charge neutrality, ions from the electrolyte diffuse toward the electrode to form a condensed layer known as the diffusion layer. This process of adsorption of charges is known as the electric double layer (EDL).

As shown in Figure 1a, the potential of the electrode decreases as the distance between the electrode and the electrolyte increases. The total capacitance of the electrode is the series combination of the capacitances that correspond to the Helmholtz layer (C_H) and the diffusion layer (C_D) as described by the relation (1),[61,62]

$$\frac{1}{C_{DL}} = \frac{1}{C_H} + \frac{1}{C_D} \quad (1)$$

When the potential is applied to the SC device, cations are adsorbed on the negatively charged electrode and the anions are adsorbed on the positively charged electrode.

On the other hand, the pseudocapacitance involves a faradaic charge storage mechanism. It has been observed that the capacitive feature of the electrode is originated from the following faradaic mechanisms, i) underpotential deposition, ii) redox pseudocapacitance and iii) intercalation pseudocapacitance.[63] In the underpotential deposition, metal ions construct an adsorbed monolayer on the surface of other metals with higher redox potential. The redox pseudocapacitance is mostly observed in aqueous electrolytes when ions are electrochemically absorbed onto the near-surface of electrode materials with faradaic charge transfer, for instance, MnO_2 and RuO_2 (Figure 1b). The intercalation pseudocapacitance arises owing to the intercalation of ions into the tunnels or layers of material along with a faradaic charge-transfer reaction, interestingly, the crystallographic phase of the materials doesn't change (Figure 1c). ZIBs are assembled using a zinc metal anode, an aqueous electrolyte such as $ZnSO_4$, and a cathode for Zn^{2+} intercalation/de-intercalation (Figure 1d). The charge storage mechanism of ZIB is quite similar to lithium-ion batteries

Ajay Jagadale is a DST INSPIRE Faculty in the Department of Electrical and Electronic Engineering at SASTRA Deemed to be University, India. He completed his master's and a Ph.D. degree in physics at Shivaji University, India. He is a recipient of the prestigious JSPS (Japan Society for Promotion of Science) postdoctoral and DST INSPIRE faculty fellowships. He worked at Kettering University, Flint, USA as a postdoctoral fellow. He leads a research group focused on the synthesis of novel electrode materials for supercapacitor and electrocatalytic applications.

Ravichandran Chitra Rohit received his master's degree from Bharathiar University in 2018. He is currently working as a Junior research fellow and research scholar at SASTRA Deemed to be University, India (with Dr. Ajay Jagadale). His research topic is synthesis of layered nanostructured materials for the supercapacitor application.

Dr. Surendra Krushna Shinde is currently working as an Assistant Professor in the Department of Biological and Environmental Science, Dongguk University, South Korea since March 2016. Dr. Surendra received his Ph.D. and M.Sc. from Shivaji University, Kolhapur, India, in 2015 in the Modern Optics. His research interest is motivated by the electrochemical synthesis of nanostructured materials and their applications in solar cells, electrocatalysis, supercapacitors, biocompatibility and antibacterial activity.

Prof. (Dr.) Dae-Young Kim is currently working as a Professor in the Department of Biological and Environmental Science, Dongguk University, South Korea. Prof. Kim received his Ph.D. from the University of Tokyo. Recently, he leads a research group focused on the synthesis of Biomaterials Science; Carbonization characteristics of holocellulose from green wood, development of multi-functional carbon materials, supercapacitor and electrocatalytic applications.

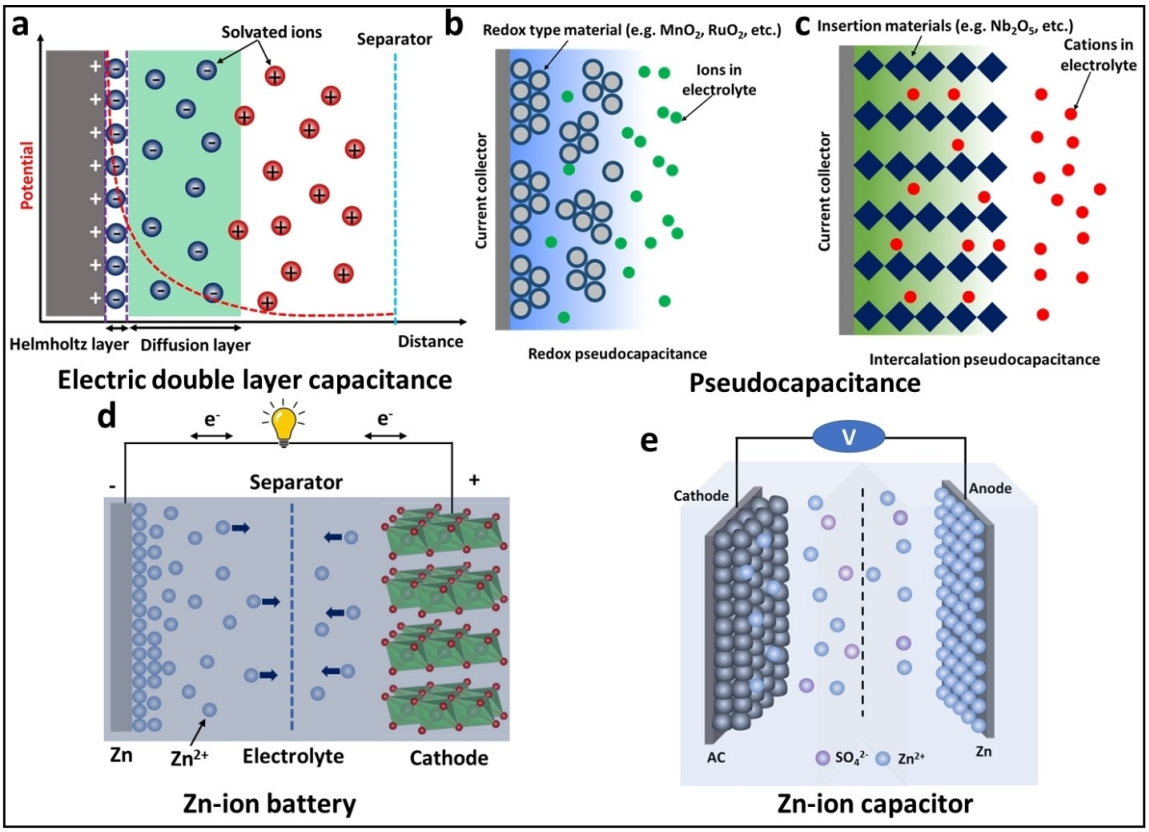

Figure 1. Schematic of storage mechanism of (a–c) SC, (d) ZIB and (e) ZIC.

and it is mostly based on the reversible Zn^{2+} insertion/extraction in the host materials. During discharging, Zn^{2+} ions are intercalated into the cathode and undergo a reduction reaction, leading to a decrease in the oxidation state. While during charging, the cathode releases Zn^{2+} by oxidizing Zn species which were already intercalated. The process can be described using the following electrochemical reactions,[64]

$$\text{Anode}: \quad Zn \leftrightarrow Zn^{2+} + e^{-} \tag{2}$$

$$\text{Cathode}: \quad M + xZn^{2+} + 2xe^{-} \leftrightarrow Zn_xM \tag{3}$$

$$\text{Overall}: \quad xZn + M \leftrightarrow Zn_xM \tag{4}$$

where M is cathode materials. Materials with adequate lattice space can be considered ideal cathodes for ZIB, for instance, tunnel or layered structures.

As shown in Figure 1e, The ZIC is fabricated using high surface area activated carbon as a cathode, Zn metal foil as an anode and aqueous $ZnSO_4$ as an electrolyte. Unlike lithium-ion capacitors, the charge storage mechanism of ZIC is slightly complex as discussed below. The Zn anode reaction involves stripping/plating of Zn/Zn^{2+} as given by the equation (5),

$$Zn \leftrightarrow Zn^{2+} + 2e^{-} \tag{5}$$

The adsorption/desorption happens on the cathode which is generally prepared with a high specific surface area and suitable pore size distribution, assuring the adsorption/desorption of both Zn^{2+} and SO_4^{2-} ions from the electrolyte. When the operating voltage of ZIC is lower than the potential of zero charge, (psz) (a potential at which differential capacitance is minimum), the adsorption/desorption of Zn^{2+} ions is the dominant process, while for potential higher than the psz, the adsorption/desorption of SO_4^{2-} ions take place.[65] Apart from the above-mentioned mechanisms, the specific capacity also originates from the precipitation/dissolution reaction of $Zn_4SO_4(OH)_6 \cdot 5H_2O$ on both electrodes.[66] We have classified the literature of ZIC based on the developmental efforts made in anode, cathode and electrolyte materials as shown in Figure 2. The electrode engineering, device configuration, energy storage mechanism and electrochemical performance of ZIC have been discussed.

3. Materials development

3.1. Development in anode materials

Recently, a significant amount of research work has been performed on anode materials of ZICs including Zn metal foil, V_2O_5, TiS_2 and activated carbon. Much work has been devoted

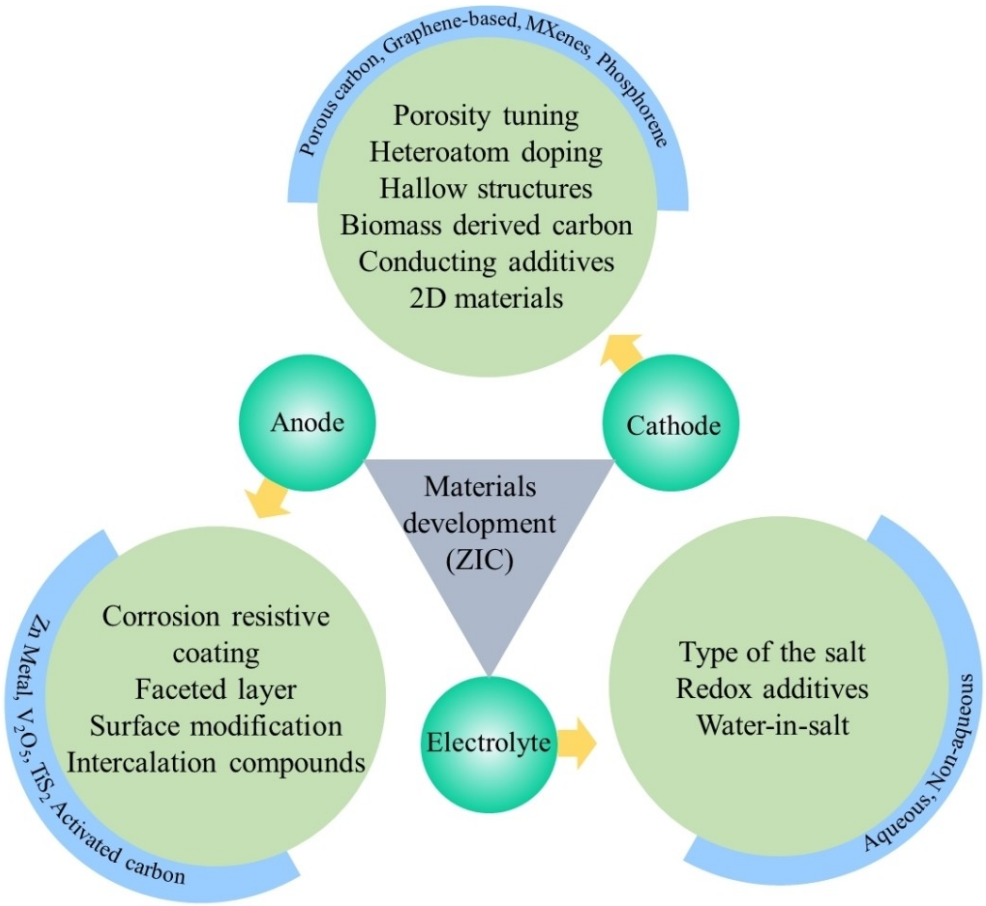

Figure 2. Schematic of materials development with different strategies of ZIC.

to addressing issues related to planar Zn anode which is mainly suffered from dendrites formation and side reactions by applying corrosion resistive coating, faceted layer and surface modification. Besides, novel anode materials have been discovered and successfully employed including 2D materials and intercalation compounds. Imperative contributions toward improving ZIC performance have been discussed below.

3.1.1. Zn-metal

The Zn metal has been considered as an ideal anode material for ZIC owing to several exceptional properties, particularly high theoretical capacity (823 $mAh \cdot g^{-1}$), relatively low redox potential (−0.76 V vs. SHE), high safety, nontoxicity and low cost. However, the wide-ranging application of ZIC is mainly hindered by the dendrites formation and side reactions at the Zn/electrolyte interface. Moreover, the Zn metal is not adequately stable in the aqueous electrolyte owing to the dissolved O_2, free water and low stripping/plating efficiency. The unwanted spontaneous side reactions lead to corrosion of the Zn metal anode, deteriorating the overall performance of the cell. In addition, the gas evolution during the cycling increases the inner pressure of the cell, creating safety issues. These issues can be rectified by applying corrosion resistive coating on the Zn anode. For instance, Han et al.[67] used Indium as a corrosion inhibitor and nucleating agent to stabilize Zn metal in an aqueous electrolyte. The corrosion reaction was examined by cycling symmetric coin cells made of two identical bare Zn or Zn|In electrodes. As shown in Figure 3a, for the bare Zn cell, gas evolution was observed on the Zn surface, however, it was observed to be suppressed on the Zn|In surface. The Zn–In//AC ZIC showed a maximum energy density of 70.4 $Wh \cdot kg^{-1}$ at a power density of 85.4 $W \cdot kg^{-1}$ and a long cycle life up to 5000 cycles at 2 $A \cdot g^{-1}$ (Figure 3b–3c). The authors provided the experimental evidence for the formation of insoluble zinc hydroxide sulfate hydrates ($Zn_4SO_4(OH)_6 \cdot xH_2O$) as by-products during the corrosion process and proved the dual functionality of the In layer.

The dendrites formation can be suppressed by regulating Zn deposition through the construction of artificial layers in between Zn metal and the electrolyte. Zhang et al.[68] coated a faceted TiO_2 on the Zn foil via blade coating method to suppress dendrite formation and make uniform Zn deposition. Prior to this, the density functional theory (DFT) calculation was performed to predict the facets of TiO_2 with lower Zn affinity. The (001) faceted TiO_2 was coated on the Zn foil and its electrochemical performance was compared with bare Zn foil

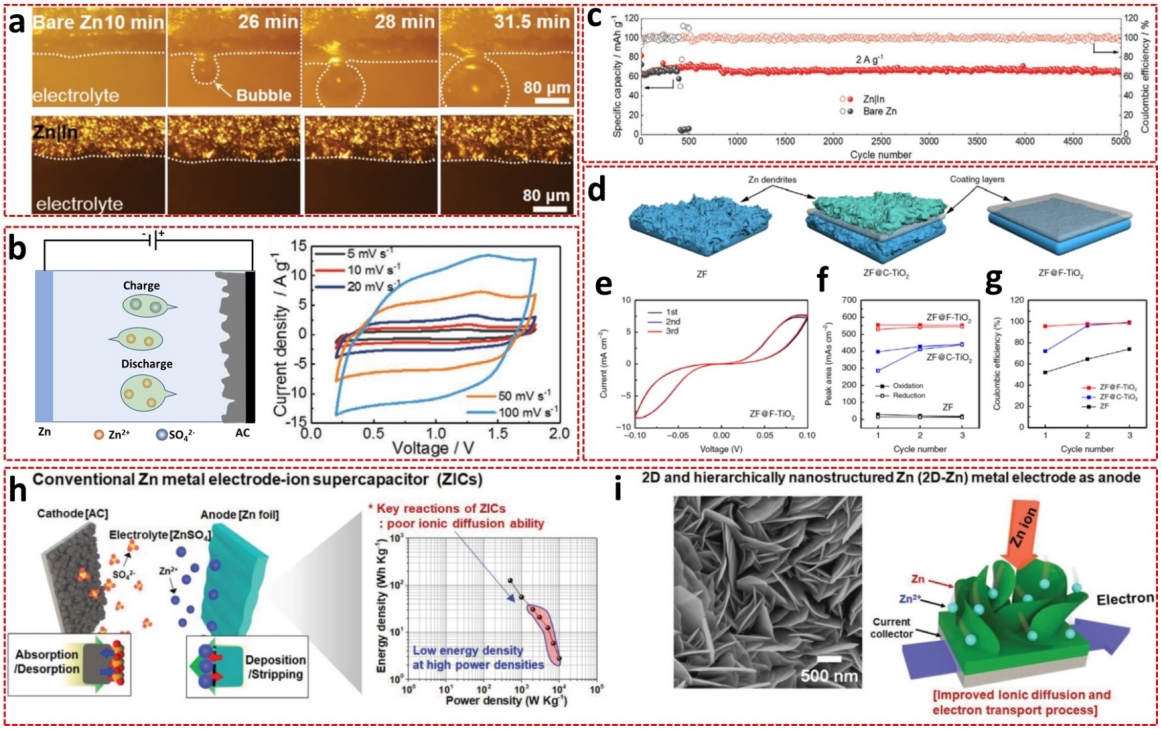

Figure 3. (a) Optical microscopic images during the gas evolution of bare Zn and Zn–In anodes in the aqueous $ZnSO_4$ electrolyte at 10 $mA \cdot cm^{-2}$. (b) CV curves of the Zn | In//AC ZIC at various scan rates. (c) The cycling stability and coulombic efficiency of bare Zn and Zn | In//AC ZIC, (a–c) reproduced with permission from the ref. [67]. Copyright 2020, Wiley-VCH (d) Schematic of Zn plating process with different coating layers. (e) CV curves of cell with faceted TiO_2 coated Zn anode at 1 $mV \cdot s^{-1}$. (f) Variation of peak area and cycle number. (g) Coulombic efficiency, (d–g) reproduced with permission from the ref. [68]. Copyright 2020, Springer Nature (h) Schematic of planar Zn based ZIC and Ragone plot. i) SEM and schematic of 2D Zn anode, (h–i) reproduced with permission from the ref. [71]. Copyright 2020, Wiley-VCH.

and the commercial TiO_2-coated Zn anodes. Figure 3d shows the Zn plating procedure for different Zn anodes. Bare Zn anode could not prevent the dendrite formation, whereas, on commercial TiO_2-coated Zn anode, Zn was grown on the surfaces of TiO_2 with higher Zn affinity. Interestingly, the 001 faceted TiO_2 coating proved to be an excellent protective layer since the Zn plating reaction was confined under this layer. This anode showed excellent Zn stripping/plating reversibility and interfacial activity when compared with other anodes (Figure 3e–3f). As shown in Figure 3g, the highest value of coulombic efficiency suggests the appreciable reversibility and uniform Zn deposition. Thus, the specific crystal orientation of TiO_2 may lead to enhanced Zn^{2+} concentration that guides uniform Zn deposition and thereby suppresses the dendrite formation. In another study, Li et al.[69] coated a non-conductive polyacrylamide (PAM)/polyvinylpyrrolidone (PVP) binary blend layer on Zn anode to prevent Zn dendrite formation and side reactions. The ZIC fabricated with PAM/PVP coated Zn anode and activated carbon (AC) cathode showed specific capacitance, energy density and power desnity of 336 $F \cdot g^{-1}$, 118 $Wh \cdot kg^{-1}$ 17.9 $kW \cdot kg^{-1}$, respectively. Interestingly, the cell demonstrated 100% capacitive retention after 6000 cycles at 15 $A \cdot g^{-1}$. Authors claimed that the superior cyclic performance is attributed to polymer coating, assisting in forming a uniform zinc deposition during the charging-discharging process. Also, it acts as an electrostatic shield layer, preventing the building up of Zn^{2+}/ electrons on the tips and impeding the growth of zinc dendrites. In another study, Dong et al.[70] used freestanding and conductive CNT scaffolds in between the Zn anode and separator for stabilizing the anode for both ZIB and ZIC. The cell with CNT scaffold-stabilized Zn anode demonstrated a small polarization potential, long cycle life and excellent rate capability. Authors claimed that the porous CNT scaffolds inhibit the formation of dendrites by maintaining a stable electric field on the Zn electrode surface and thereby regulating Zn^{2+} deposition sites.

The ZIC with flat Zn metal anode shows an inferior rate and thus the power performance due to the poor diffusion ability of the Zn electrode (Figure 3h). The diffusion pathways can be reduced by modifying or roughening and creating nanoarchitectures on the Zn surface. An et al.[71] prepared 2D hierarchically nanostructured Zn metal anode via voltage-tailored electroplating method and the morphology and structure were optimized (Figure 3i). This unique structure provided shorter diffusion paths and enhanced surface area, leading to a high-power performance of 500 $W \cdot kg^{-1}$ with an energy capability of 208 $Wh \cdot kg^{-1}$. This excellent electrochemical performance was attributed to the novel nanoarchitecture of Zn anode, facilitating numerous electrochemically active sites and effortless ionic transport. In another work, a novel chemical etching process was employed to modify the Zn surface, reducing diffusion pathways of Zn ions during the cycling.[72] The surface

modification of the Zn anode was done using the phosphoric acid (H_3PO_4) for the 0, 1, and 10 min. The anode modified at 10 min demonstrated impressive performance which was utilized for device fabrication. The ZIC cell was constructed using surface-modified Zn anode (10 min), AC cathode and 2 M $ZnSO_4$ electrolyte. This ZIC showed a maximum energy density of 125 $Wh \cdot kg^{-1}$ at a power density of 400 $W \cdot kg^{-1}$ and the capacitive retention of 99% after 2000 cycles at 5 $A \cdot g^{-1}$. The authors claimed that the improved performance is ascribed to the shorter ion diffusion pathways of the Zn anode. In another study, An et al.[73] prepared Zn anode with thin-walled architectures via the electroplating method. The electroplating was done at different voltages of 0.5, 1.0 and 1.5 V for 6 min. The ZIC was assembled using a thin-walled Zn anode (prepared at 1.0 V), AC cathode and aqueous solution of 2 M $ZnSO_4$ electrolyte. This ZIC cell demonstrated a maximum specific capacitance of 421 $F \cdot g^{-1}$ at a current density of 0.5 $A \cdot g^{-1}$ with improved rate capability by offering specific capacitance of 150 $F \cdot g^{-1}$ at a high current density of 10.0 $A \cdot g^{-1}$. The cycling stability of 99% was observed after 3000 cycles. Authors claimed that the excellent performance is attributed to the thin-walled architecture of the Zn anode, facilitating enormous electrochemically active sites and reducing ionic diffusion pathways. Liu et al.[74] fabricated ZIC using mesoporous hollow carbon spheres (MHCSs) cathode and MHCSs coated Zn foil anode. The MHCS//Zn–MHCS ZIC showed the energy density of 129.3 $Wh \cdot kg^{-1}$ at power density of 266.4 $W \cdot kg^{-1}$ with excellent cyclic stability of 96% after 10000 cycles at 1 $A \cdot g^{-1}$ in 2 M $ZnSO_4$ electrolyte. Authors claimed that the MCHSs coating on Zn anode prevents dendrites formation and directs a uniform Zn deposition process. Thus, as discussed above, most of the research efforts were made to address issues related to metal Zn anode including dendrite formation, side reactions, instability in aqueous electrolyte, corrosion, poor diffusivity, etc.

3.1.2. TiS_2

Apart from the sluggish diffusion of Zn ion, the pristine Zn metal anode has several disadvantages such as the formation of byproducts on the surface and the insufficient utilization rate of Zn metal. These issues can be addressed by preparing high capacity and rate capability intercalation anodes with appropriate potential. The graphene-like 2D-layered TiS_2 is a promising electrode material for ZIC due to its large interlayer spacing of 5.7 Å (suitable for insertion of divalent cations) and lower insertion potential of 0.3 V (vs Zn^{2+}/Zn) in an aqueous electrolyte. Wang et al.[75] synthesized 2D-layered TiS_2 with a large interlayer spacing of 5.7 Å (111) and used it as an anode in ZIC (Figure 4a–4b). The ZIC combined with an AC cathode and 2 M $ZnSO_4$ electrolyte showed a maximum specific capacitance of 249 $F \cdot g^{-1}$ at 0.2 $A \cdot g^{-1}$ and energy density of 112 $Wh \cdot kg^{-1}$ at a power density of 180 $W \cdot kg^{-1}$. Also, this ZIC demonstrated excellent cyclic stability of 92% after 5000 cycles at a current density of 2 $A \cdot g^{-1}$. A superior performance, in this case, was attributed to novel TiS_2 anode material, avoiding dendrite growth during the charging-discharging process and facilitating rapid kinetics of Zn ion.

3.1.3. AC

A few research groups focus on utilizing carbonaceous materials as anodes for ZIC. For instance, Ma et al.[76] fabricated ZIC

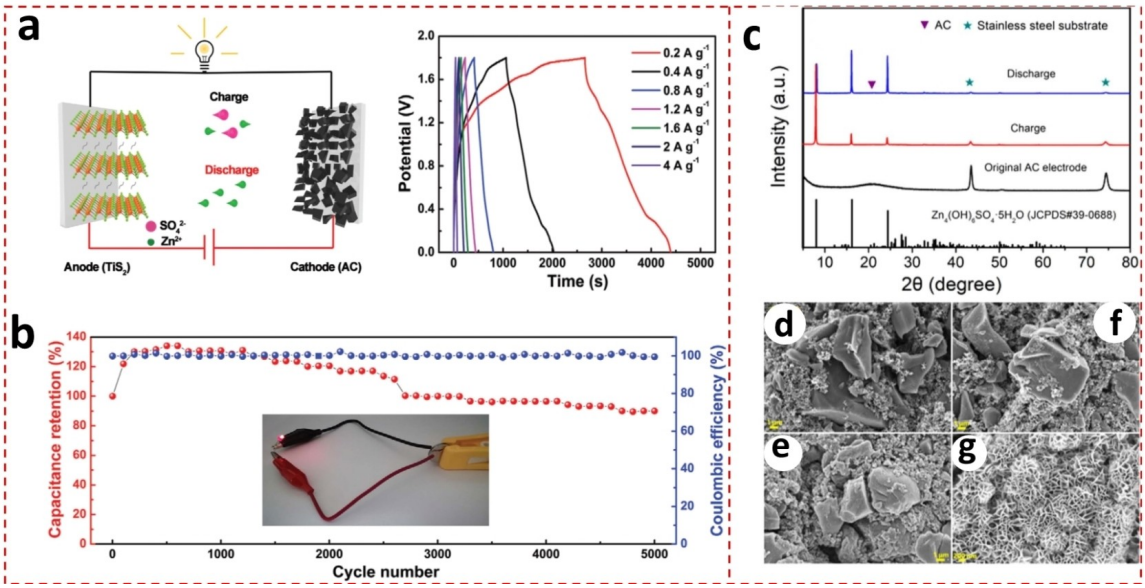

Figure 4. (a) The construction and storage mechanism and GCD curves from 0.2 to 4 $A \cdot g^{-1}$ of TiS_2//AC ZIC. (b) The stability performance of (inset: lighted LED) TiS_2//AC ZIC, (a–b) reproduced with permission from the ref. [75]. Copyright 2020, Wiley-VCH (c) XRD patterns of AC anode at charged and discharged states. (d) SEM image of original AC, (e) at discharged state (f) charged state and (g) irreversible $Zn_4(OH)_6SO_4 \cdot nH_2O$ formed on AC, (c–g) reproduced with permission from ref. [76]. Copyright 2019, Elsevier.

using AC as an anode and MnO_2 as a cathode in 2 M $ZnSO_4$ electrolyte. The AC//MnO_2 ZIC fabricated with AC to MnO_2 mass ratio of 2.5:1 showed a maximum specific capacity of 54.1 mAh·g^{-1} with an energy density of 34.8 Wh·kg^{-1}. In this work, the charging-discharging mechanism of the cell was provided. The ion adsorption/desorption occurs on the AC anode and reversible insertion/extraction of Zn^{2+} occurs on the MnO_2 cathode. The structural changes on the AC anode were investigated using *ex-situ* XRD as shown in Figure 4c. During the charging-discharging of this ZIC, the irreversible $Zn_4(OH)_6SO_4 \cdot xH_2O$ by-product was formed on both electrodes in $ZnSO_4$ aqueous electrolyte, hindering their practical applicability. The surface modification was confirmed by SEM images (Figure 4d–4f). This issue can be addressed by utilizing a chemically stable V_2O_5 cathode. In another study, the same research group fabricated ZIC using AC as an anode, V_2O_5 as a cathode and aqueous $ZnSO_4$ as an electrolyte. The optimized anode to cathode mass ratio was found to be 1:1. The AC//V_2O_5 ZIC showed a maximum specific capacity of 57.4 mAh·g^{-1} and an energy density of 34.6 Wh·kg^{-1}. Authors claimed that, in this configuration, a by-product was not formed that led to the excellent cyclic stability with a capacity retention of 97.3% after 6000 GCD cycles.[77] In most of the reports, Zn metal and surface modified Zn anode has been used for ZIC fabrication. The capacitive performance of ZIC based on different anode materials is summarized in Table 2.

3.2. Development in cathode materials

Since cathodes contribute mainly through their capacitive nature, efforts have been made to improve their specific capacitance and energy density. Works including preparation of porous and hallow structured carbon, porosity tuning, heteroatom doping, selection of different carbon sources, conducting additives, utilizing electrically conducting 2D materials, etc. have been performed as described below.

3.2.1. Porous carbon

A porous carbon cathode material has been massively studied electrode material for SC as well as ZIC due to its low cost, abundance, sustainability and high specific surface area. The commercially available AC is mostly reported cathode material which mainly suffers from its poor ionic diffusion and transport abilities owing to its microporous nature and poor wettability. An et al.[88] synthesized mesoporous carbon via dehydrogenation of polyvinylpyrrolidone (PVP) coated from the solutions of different concentrations on the commercial AC. When the concentration of PVA increases, the oxygen-containing groups in the mesoporous carbon also increase and thereby the wettability of the sample. The mesoporous carbon prepared with a PVP coating solution of 1 mM concentration showed a

Table 2. Capacitive performance of ZIC based on different anode materials reported so far.

Device configuration [Anode//cathode]	Electrolyte	Voltage range [V vs Zn/Zn2+]	Energy density [Wh.kg^{-1}]	Power density [W.kg^{-1}]	Cyclic stability [%]	Reference
PAM/PVP coated Zn//AC	3 M $Zn(CF_3SO_3)_2$	0–2.0	118	17900	100 after 6000 cycles at 15 A.g^{-1}	[69]
Surface modified Zn//AC	2.0 M $ZnSO_4$	0.2–1.8	125	400	99 after 2000 at 5 A.g^{-1}	[72]
TiS_2//AC	2 M $ZnSO_4$	0–1.8	112	180	92 after 5000 at 2 A.g^{-1}	[75]
Ag@V_2O_5//AC	3 M $Zn(CF_3SO_3)_2$	0–1.6	53.13	36.74	99 after 4000 at 1 A.g^{-1}	[78]
Zn–In//AC	2 M $ZnSO_4$	0.2–1.8	70.4	85.4	~100 after 5000 at 2 A.g^{-1}	[67]
AC//MnO_2	2 M $ZnSO_4$ + 0.5 M $MnSO_4$	0–2.0	58.6	–	93.4 after 5000 at 1 A.g^{-1}	[76]
AC//V_2O_5	2 M $ZnSO_4$	0–2.0	34.6	13000	97.3 after 6000 at 0.5 A.g^{-1}	[77]
Zn coated MCHS//MCHS	2 M $ZnSO_4$	0.2–1.8	129.3	266.3	96 after 10000 at 1 A.g^{-1}	[74]
Zn coated diamond fiber// diamond fiber	1 M $ZnSO_4$	0.2–1.8	70.7	709.0	89.9 after 10000 at 1 A.g^{-1}	[79]
HMCS//HMCS	1 M Na_2SO_4 + 2 M $ZnSO_4$	0–1.6	75.4	160	99.4 after 2500 at 2 A.g^{-1}	[80]
MWCNTs–RGO–Zn// MWCNTs–RGO	Poly(vinyl alcohol) (PVA)/$Zn(CF_3SO_3)_2$	0–1.8	13.1 mWh.cm^{-3}	1433.2 mW.cm^{-3}	80.8 after 10000 at 3.1848 A.cm^{-3}	[81]
MXene@COC//δ-MnO2@CAC	23 g $ZnSO_4$ + 0.676 g $MnSO_4$	0–1.9	90	239	80.7 after 16000 at 5.05 A.g^{-1}	[82]
Ti_3C_2Tx//MnO_2–CNTs	2 M $ZnSO_4$ + 0.1 M $MnSO_4$	0–1.9	98.6	77.5	83.6 after 15000 at 5.224 A.g^{-1}	[83]
Zn//AC	2 M $ZnSO_4$	0.2–1.8	84	14900	91 after 10000 at 1 A.g^{-1}	[84]
Zn//AC	1 M $Zn(CF_3SO_3)_2$ in acetonitrile	0–1.8	52.7	1725	91 after 20000 at 2 A.g^{-1}	[85]
Zn//Graphite	1 M ($Zn(OAc)_2$ in choline acetate (70%) + water (30%) (ionic liquid)	0–1.8	53	145	86 after 1000 at 0.5 A.g^{-1}	[86]
Zn//AC	2 M $ZnSO_4$	0.2–1.4	–	–	93 after 5000 at 5 A.g^{-1}	[87]

high surface area (2527 $m^2 \cdot g^{-1}$) and large pore volume (2.7 $cm^3 \cdot g^{-1}$). The ZIC fabricated with Zn anode showed a maximum energy density of 188 $Wh \cdot kg^{-1}$ at a power density of 533 $W \cdot kg^{-1}$ along with the cyclic stability of 94% after 1500 cycles at 0.5 $A \cdot g^{-1}$. This mesoporous carbon showed high-rate capability, excellent ionic diffusivity and long cycle life.

Moreover, the introduction of heteroatoms or dopants can effectively increase the electrical conductivity as well as the wettability. Lee et al.[89] prepared P and B doped AC via a one-pot doping calcination process for ZIC. The assembled cell with Zn foil anode and 2 M $ZnSO_4$ electrolyte showed a maximum specific capacity of 169.4 $mAh \cdot g^{-1}$ at 0.5 $A \cdot g^{-1}$ with appreciable rate capability and larger capacity retention of 88% after 30000 cycles at 10 $A \cdot g^{-1}$. The superior performance was attributed to the synergic effect of P and B co-doping, offering exceptional diffusion kinetics and charge-transfer process. Recently, boron-doped diamond (BDD) has attracted great attraction as a promising capacitive electrode owing to its wide potential window, long cycle life and environmental friendliness. Jian et al.[79] prepared carbon/Ti/BDD fibers hybrid cathode for ZIC by combing different physical and chemical methods including sputtering, chemical vapor deposition and electrodeposition (Figure 5a). In their work, diamond fibers with different grain sizes were tested for electrochemical performance, interestingly, the grain size of 200–300 nm demonstrated the highest capacitive performance. The ZIC was assembled with zinc nanosheet coated diamond fibers anode and 1.0 M $ZnSO_4$ electrolyte that showed a maximum energy density of 70.7 $Wh \cdot kg^{-1}$ at a power density of 709.0 $W \cdot kg^{-1}$. Furthermore, a flexible ZIC was fabricated using gelatin and its mechanical properties were tested at different bending angles as shown in Figure 5b. Interestingly, the change of capacitance value was less than 2.43% after 1000 bending cycles, indicating its promising role in wearable electronics. In another work, Wang et al.[90] prepared S-doped 3D porous carbons via potassium thioacetate activation technique and used as a cathode in ZIC. The S-doped 3D porous carbon was prepared via pyrolysis at 800 °C showed an excellent specific capacity of 203.3 $mAh \cdot g^{-1}$. The Zn//S-doped porous carbon cell demonstrated a maximum energy density of 162.6 $Wh \cdot kg^{-1}$ at a power density of 160 $W \cdot kg^{-1}$. Authors claimed that the enhanced performance is attributed to a unique 3D architecture with a large specific surface area and a particular amount of sulfur (0.88–3.60 at%).

Recently, hollow bowl-like carbon (HBC) has been considered the most prominent cathode material for ZIC owing to its enhanced packing density, sturdy structural stability and superior electrical conductivity. Fei et al.[91] fabricated ZIC using HBC as a cathode, Zn foil as an anode and aqueous $ZnSO_4$ solution as the electrolyte. As shown in Figure 5c, the hard template for HBC was synthesized using resorcinol (R), formaldehyde (F), and tetraethyl orthosilicate (TEOS). The mass ratio of R, F, and TEOS was tuned to achieve an HBC or hollow carbon sphere with different shell thicknesses. As shown in Figure 5d, the energy is stored via reversible adsorption/desorption (SO_4^{2-} ions) on the HBC cathode and plating/stripping (Zn^{2+} ions) on the Zn anode. The Zn//HBC ZIC demonstrated a specific capacity of 95.4 $mAh \cdot g^{-1}$ at 0.1 $A \cdot g^{-1}$ along with the cyclic stability of 98% after 1000 cycles at 1 $A \cdot g^{-1}$. Authors claimed that the high performance is ascribed to the abundant meso-channels and high accessible surface area. In another study, Chen et al.[80] prepared hollow mesoporous carbon spheres (HMCS) cathode via carbonization and alkaline washing of SiO_2@C nanospheres. The ZIC was combined with two HMCS electrodes and Zn ion-containing electrolyte

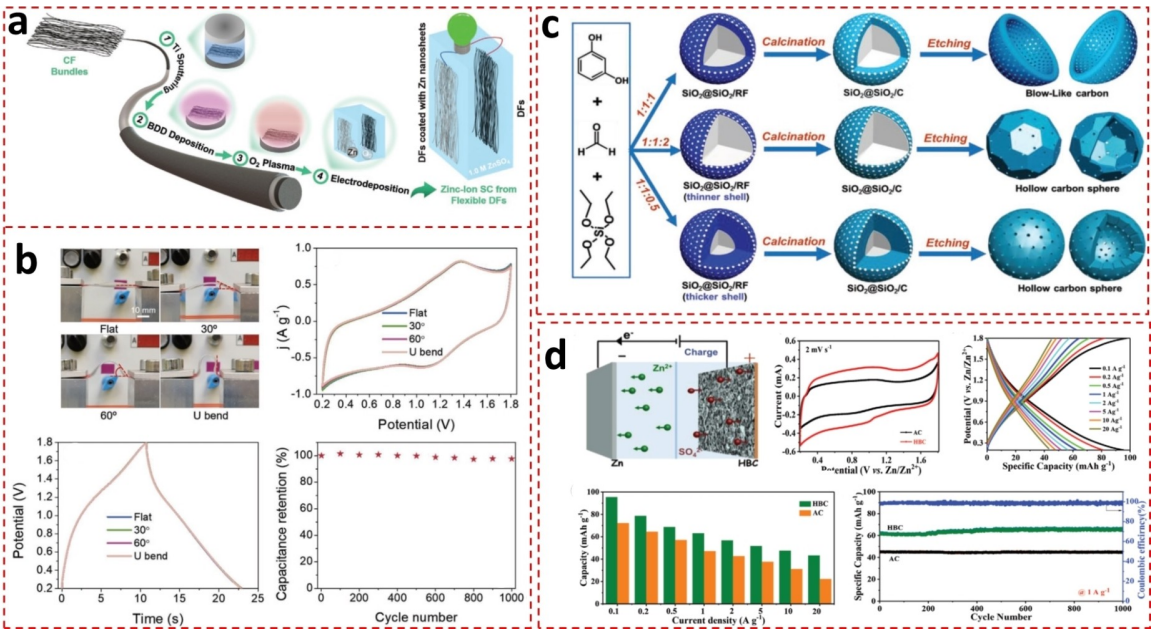

Figure 5. (a) Schematic of preparation procedure of flexible diamond fibers and the fabrication of ZIC. (b) Flexibility studies of diamond fiber-based ZIC, (a–b) reproduced with permission from ref. [79]. Copyright 2020, Wiley-VCH (c) Schematic formation of hollow bowl-like carbon (HBC) and hollow carbon sphere (HCS). (d) Electrochemical performance of Zn//HBC ZIC, reproduced with permission from the ref. [91]. Copyright 2020, Wiley-VCH.

that showed high specific capacitance of 212.1 $F \cdot g^{-1}$ at 0.2 $A \cdot g^{-1}$, energy density of 75.4 $Wh \cdot kg^{-1}$ at a power density of 0.16 $kW \cdot kg^{-1}$, and the capacitance retention of 99.4% after 2,500 cycles at 2 $A \cdot g^{-1}$.

The capacitive performance of the cathode materials can be improved by introducing mesopores and macropores to the electrode materials. Mesopores facilitate the diffusion channels to the electrolytic ions and macropores act as a reservoir for the electrolyte. These types of pores are imperative to achieve excellent energy storage performance. Normally, this can be done by using soft and hard templates and by optimizing the chemical activation process which may add fabrication cost. Recently, naturally available bio-waste has been efficiently used for the derivation of high-quality carbon with useful and hierarchical pore structures. For instance, Jiang et al.[92] prepared mesoporous carbon with high specific surface area (2807 $m^2 \cdot g^{-1}$) and large pore volume (2.558 $cm^3 \cdot g^{-1}$) via KOH activation of polyurethane foam filler. In their research, the ratio of the pre-carbonized precursor to KOH was varied from 1 to 3. The ZIC fabricated with Zn anode and the mesoporous carbon activated with ratio 3 showed the maximum energy density of 92.7 $Wh \cdot kg^{-1}$ at 179 $W \cdot kg^{-1}$. The cyclic stability of the device was obtained nearly 100% after 10000 cycles at 2 $A \cdot g^{-1}$. The authors claimed that this mesoporous carbon electrode provides sufficient ion diffusion channels for the adsorption/desorption of $(CF_3SO_3)^-$ ions, leading to a fast charge transfer kinetics during charge-discharge. Zeng et al.[93] fabricated aqueous as well as micro-ZIC using Kelp-derived carbon cathode and Zn foil anode via 2 M $Zn(CF3SO_3)_2$ aqueous and polyacrylamide-based polymer gel electrolytes, respectively. The aqueous ZIC showed a maximum specific capacity of 196.7 $mAh \cdot g^{-1}$ at 0.1 $A \cdot g^{-1}$ and an energy density of 111.5 $Wh \cdot kg^{-1}$ at a power density of 1300 $W \cdot kg^{-1}$. The flexible micro-ZIC demonstrated a high areal capacity of 10.28 $\mu Ah \cdot cm^{-2}$ at a current density of 0.1 $mA \cdot cm^{-2}$. The micro-ZIC exhibited an areal energy density of 8.2 $\mu Wh \cdot cm^{-2}$ at a power density of 40 $\mu W \cdot cm^{-2}$. In another study, Li et al.[94] fabricated ZIC using biowaste (pencil shavings)-derived porous carbon cathode, Zn foil anode and 1 M $Zn(CF_3SO_3)_2$ electrolyte. The ZIC demonstrated a high energy density of 147.0 $Wh \cdot kg^{-1}$ at 136.1 $W \cdot kg^{-1}$ along with the cycling stability of 92.2% after 10000 cycles at a current density of 10 $A \cdot g^{-1}$. Moreover, the anti-freezing hydrogel electrolyte based on polyvinyl alcohol, ethylene glycol and $Zn(CF_3SO_4)_2$ salt was employed for the fabrication of the quasi-solid-state hybrid supercapacitor that showed its smooth operation even at a relatively low temperature of −15 °C.

The energy density of the ZIC can be effectively increased by incorporating faradaic redox materials on the carbon surface. Yin et al.[95] synthesized porous carbon via pyrolysis of pyromellitic acid tetra-potassium salt followed by acid etching. The ZIC was assembled with this porous carbon cathode, zinc metal foil anode and 3 M $Zn(ClO_4)_2$ aqueous electrolyte. The device demonstrated a maximum energy density of 104.8 $Wh \cdot kg^{-1}$, a power density of 48.8 $kW \cdot kg^{-1}$ and cyclic stability of 99.2% after 30000 cycles. This excellent performance was attributed to reversible redox reactions of hydrogen and oxygen present on the carbon surface. To get benefited from the pseudocapacitive oxygen-containing functional groups on the carbon surface, Zheng et al.[45] prepared oxygen-rich 3D porous carbon for ZIC. The ZIC combined with Zn coated carbon cloth anode showed an excellent specific capacity of 132.7 $mAh \cdot g^{-1}$ and energy density of 82.36 $Wh \cdot kg^{-1}$ along with an acceptable capacity retention of 87.6% after 10,000 cycles at 1.0 $A \cdot g^{-1}$. It has been claimed that oxygen functional groups facilitate pseudocapacitance and exceptional pore structure bestows the rapid electrochemical kinetics.

3.2.2. Graphene-based

Graphene and graphene-based materials have been considered excellent capacitive electrodes for energy storage applications. The graphene exhibits interesting properties such as large theoretical specific surface area, good electronic conductivity, and exceptional mechanical strength. However, the irreversible π-π restacking of graphene sheets hinders their potential application in SCs. There are several ways of avoiding this restacking, for example, Zhu et al.[96] synthesized graphene hydrogel by controlling the swelling of graphene oxide films. They modified the acting forces such as van der Walls, hydrogen bonding and electrostatic repulsion via hydrothermal treatment (Figure 6a). The hydrothermal pretreatment done at 120 °C for 60 min was found optimum for graphene hydrogel preparation. The ZIC fabricated with Zn anode and above optimized graphene hydrogel cathode showed a maximum energy density of 76.2 $Wh \cdot kg^{-1}$ and the capacity retention of 90% after 10,000 GCD cycles (Figure 6b). The best performance in the present case is attributed to the hierarchical porous structure of the graphene hydrogel films, facilitating ions diffusion and reduced internal impedance of the cell. Another way of avoiding π-π restacking is to prepare graphene-based composites using nanostructured materials such as carbon nanotubes, metal oxide nanoparticles, etc. Recently, Ni et al.[97] prepared multiwalled carbon nanotubes (MWCNTs)–RGO hybrid fiber electrodes for ZIC (Figure 6c). In their research, the molar ratios between MWCNTs and RGO were varied from 1:4, 1:8 and 1:16. The composite prepared at a 1:4 ratio showed excellent capacitive performance. The fiber ZIC was fabricated using MWCNTs–RGO hybrid fiber as a cathode, MWCNTs–RGO–Zn hybrid fiber as an anode, and poly(vinyl alcohol) (PVA)/$Zn(CF_3SO_3)_2$ aqueous gel as electrolyte. The maximum areal energy and power densities were obtained as 13.1 $mWh \cdot cm^{-3}$ and 1433.2 $mW \cdot cm^{-3}$ along with the cyclic stability of 80.8% after 10000 cycles. This flexible SC was capable of self-healing as indicated in Figure 6d. The gel electrolyte was simply stuck together after being fully separated. Interestingly, after healing, the electrolyte bears the weight up to 50 g, demonstrating superior self-healing capability of the fiber ZIC. Also, this fiber ZIC offered 70.5% of capacitance retention after fifth self-healing (Figure 6e). Thus, this type of ZIC will have favorable role in wearable electrons. In another study, Tian et al.[49] fabricated ZIC using zinc as an anode, oxidized carbon nanotubes as a cathode and zinc sulfate

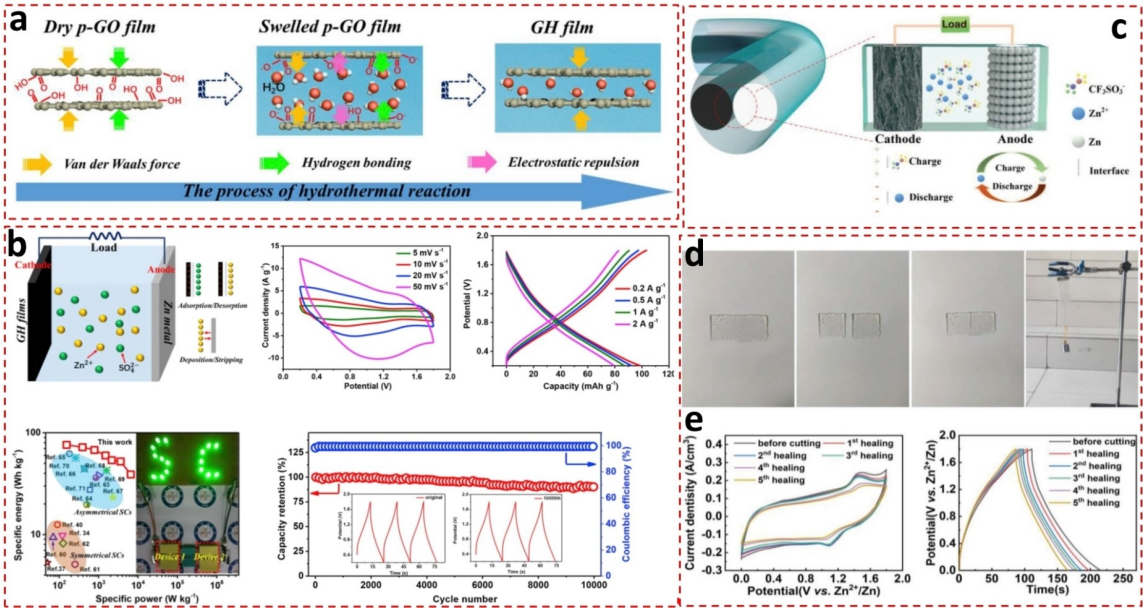

Figure 6. (a) Schematic of interlayer space evolution of graphene films. (b) Charge storage mechanism and electrochemical performance of Zn//graphene hydrogel ZIC, (a–b) reproduced with permission from the ref. [96]. Copyright 2020, Elsevier (c) Schematic of MWCNTs–RGO based ZIC with storage mechanism. (d) photographs during self-healing process of gel electrolyte, (e) CV and CGD curves of ZIC at different healing times, (c–e) reproduced with permission from the ref. [97]. Copyright 2020, Wiley-VCH.

as an electrolyte. The reaction mechanism of oxidized carbon nanotubes involves reversible faradaic reactions, leading to an excellent value of areal capacitance of 20 $mF \cdot cm^{-2}$ in the potential window of 0–1.8 V at 10 $mV \cdot s^{-1}$ along with a cyclic life of 5000 cycles.

3.2.3. MXene

MXenes are a class of two-dimensional inorganic compounds, consisting of few atoms of thick layers of transition metal carbides, nitrides, or carbonitrides. They are mainly prepared by etching a MAX ($M_{n+1}AX_n$, where M: early transition metal, A: element from group 13 or 14, X: C and/or N, and n = 1–4) phase using strong etching solutions containing a fluoride ion (F^-) such as hydrofluoric acid (HF). The accordion-like Ti_2CT_X MXene (T_X: –OH, =O, and –F) has been proven to be an effective electrode material for energy storage application owing to its high conductivity and good hydrophilicity. However, inadequate interlayer spacing, non-preferential distribution and spontaneous restacking of nanosheets during the electrode fabrication limit their potential application in ZIC. The vertically arranged nanosheets are highly desirable that not only assist for ion shuttle but also reduces the ion transport path. Inspired by this thought, Li et al.[98] prepared a core-shell Ti_2CT_X/C sphere with Ti_2CT_X vertically coated on the carbon spheres and used as a cathode for ZIC (Figure 7a). To enhance the interlayer spacing of the nanosheets, the Sn^{4+} pre-intercalation was done. The ZIC combined with a Zn anode showed excellent cycle life of up to 12500 cycles and a maximum specific capacity of 138 $mAh \cdot g^{-1}$ at 0.1 $A \cdot g^{-1}$ (Figure 7b). The authors claimed that superior performance is the consequence of enhanced ion transportation and reaction kinetics. In another work, Wang et al.[99] prepared porous 3D $Ti_3C_2T_x$–GO aerogels cathode for ZIC. This structure not only avoids restacking of $Ti_3C_2T_x$ nanosheets but also facilitates high electrical conductivity and wettability. The ZIC was fabricated using a zinc foil anode that showed excellent specific capacitance of 128.6 $F \cdot g^{-1}$ at 0.4 $A \cdot g^{-1}$ and a high energy density of 34.9 $Wh \cdot kg^{-1}$ at a power density of 279.9 $W \cdot kg^{-1}$. The ZIC also demonstrated outstanding cycling stability (75000 cycles at 5 $A \cdot g^{-1}$) and coulomb efficiency (100%). Authors claimed that the appropriate amount of MXenes in the $Ti_3C_2T_x$–GO composite enhances the conductivity and the wettability, leading to superior electrochemical performance. However, the excess amount of MXene deteriorates the performance by blocking the ionic transport during charging-discharging. Yang et al.[100] fabricated degradable and anti-self-discharge ZIC using Zn@Ti_3C_2 anode, Ti_3C_2 film cathode, and a gelatin-based gel electrolyte. This ZIC can be degraded within 8 days and shows cyclic stability of 82.5% after 1000 cycles along with a rate capability of 91.6% at 3 $A \cdot g^{-1}$. Also, the ZIC exhibited the lowest self-discharge rate of 6.4 $mV \cdot h^{-1}$. The improved anti-self-discharge property is attributed to the static electricity immune mechanism.

3.2.4. Phosphorene

Phosphorene is a two-dimensional, highly stable allotrope of phosphorous consisting of a single layer of layered black phosphorous. This few-layer phosphorene (FLP) has demonstrated great potential as a capacitive electrode in electro-

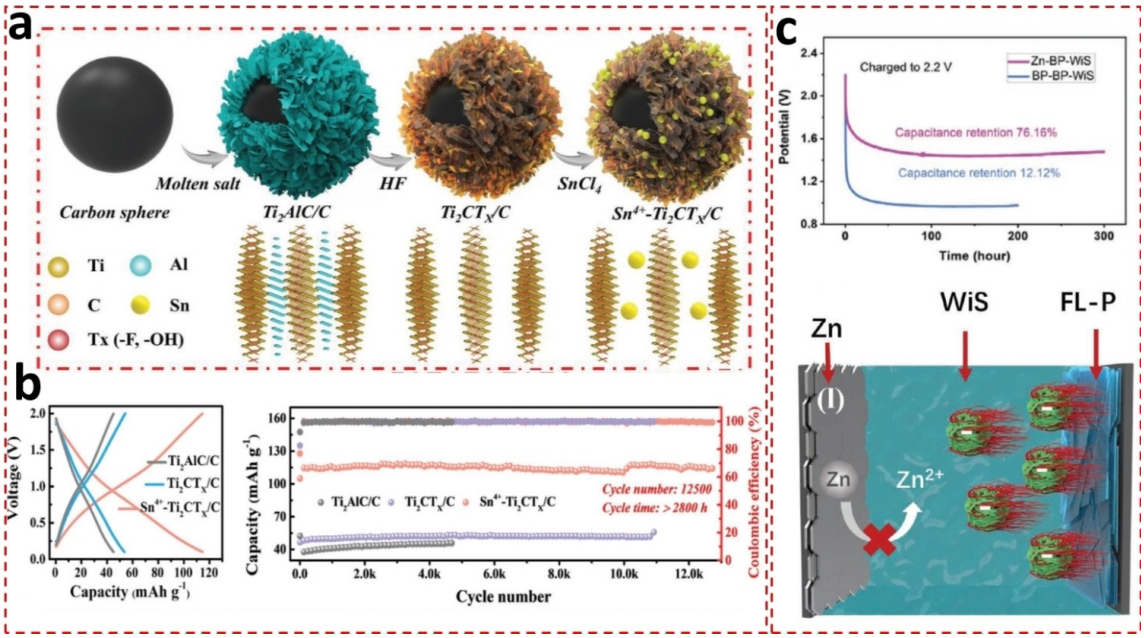

Figure 7. (a) Formation process of core-shell Sn^{4+}-Ti_2CT_X/C sphere. (b) GCD curves and stability performance of Ti_2AlC/C, Ti_2CT_X/C, and Sn^{4+}-Ti_2CT_X/C electrodes at 0.5 $A \cdot g^{-1}$, (a–b) reproduced with permission from the ref. [98]. Copyright 2020, Wiley-VCH (c) Self-discharge curves of Zn//black phosphorous (WiS) and black phosphorous//black phosphorous (WiS) and schematic of few-layer phosphorene-based ZIC in a charged state, reproduced with permission from the ref. [101]. Copyright 2020, Wiley-VCH.

chemical energy storage devices owing to its high specific surface area, mechanical robustness, and excellent carrier mobility ($\approx 10\,000\ cm^2 \cdot V^{-1} s^{-1}$). Huang et al.[101] recently prepared the FLP through the electrochemical exfoliation of black phosphorous and used as a cathode in ZIC. Two types of ZICs were fabricated by using 'water in salt' (WiS) and propylene carbonate (PC)-based electrolytes. The ZIC with WiS electrolyte showed a high capacitance of 304 $F \cdot g^{-1}$ at a current density of 0.2 $A \cdot g^{-1}$. The ZIC with PC-based electrolyte delivered a capacitance of 363.9 $F \cdot g^{-1}$ at a current density of 0.2 $A \cdot g^{-1}$. Moreover, the self-discharge characteristics of these two devices were studied. The ZIC with WiS electrolyte showed excellent anti-self-discharge property with capacitance retention of 76.16% after resting for 300 h (Figure 7c). However, ZIC with PC-based electrolyte showed capacitance retention of only 12.12% after a rest of 200 h. The superior anti-self-discharge property is attributed to the high concentration of salt that may inhibit the diffusion of ions.

3.2.5. Metal oxides

Apart from the above-mentioned cathode materials, metal oxides have also shown their capability as a cathode in ZIC because of their pseudocapacitive charge storage mechanism. Dong et al.[102] prepared amorphous $RuO_2 \cdot H_2O$ cathode for ZIC, that offers rapid and long life Zn^{2+} storage. The Zn//$RuO_2 \cdot H_2O$ ZIC showed stable working in the voltage window of 0.4–1.6 V and delivered a discharge capacity of 122 $mAh \cdot g^{-1}$. The cell could rapidly charge and discharge within 36 s and offered an impressive power density of 16.74 $kW \cdot kg^{-1}$, an energy density of 82 $Wh \cdot kg^{-1}$ and long cycle life of up to 10,000 cycles. The kinetic analysis suggests the pseudocapacitive nature of $RuO_2 \cdot H_2O$ cathode. Therefore, it is seen from the literature that much effort has been made on improving the capacitive performance of cathode materials. The storage performance of ZICs fabricated through different cathodes has been summarized in Table 3.

3.3. Electrolytes

Although an electrolyte is one of the important parts of ZIC, there have been very few researches that focus on electrolyte systems. In most of the reported work, aqueous solutions of either $ZnSO_4$ or $Zn(CF_3SO_4)_2$ are used as an electrolyte. In such electrolytes, when Zn salt is dissolved in the solution, Zn solvated ions are formed. Interestingly, the diameters of the bare Zn^{2+} and solvated Zn($[Zn(H_2O)_6]^{2+}$) ions are around 1.48 and 8.60 Å, respectively. This enlarged diameter of solvated Zn ions cannot access the inner microporous surface of the carbon material, limiting the energy storage capacity. As validated by Wang et al.,[120] the coordination of Zn^{2+} depends on the counter anions used in the electrolyte. They studied the effect of different salts in the electrolyte on the storage performance of ZIC formed of Zn metal anode and AC cathode. It has been observed that the ZIC with $ZnCl_2$ salt as an electrolyte displayed maximum energy density when compared with other electrolyte systems. From DFT calculations, it is found that the desolvation energies of Cl^- containing $[ZnCl]^+(H_2O)_{n-1}$ (n = 6–1)

Table 3. Capacitive performance of ZIC based on different cathode materials reported so far.

Device configuration [Anode//cathode]	Electrolyte	Voltage range [V vs Zn/Zn^{2+}]	Energy density [$Wh.kg^{-1}$]	Power density [$W.kg^{-1}$]	Cyclic stability [%]	Reference
Zn//g-C3N4@rGO/FTO	2 M $ZnSO_4$	0.2–1.0	0.668	1.625	90.2 after 1000 at 500 $mV.s^{-1}$	[103]
Zn//graphene hydrogel (GH)	2 M $ZnSO_4$	0.2–1.8	52.2	3602	~100 after 10000 at 15 $A.g^{-1}$	[96]
Zn//Kelp carbon	2 M $Zn(CF_3SO_3)_2$	0.1–1.7	111.5	1300	89 after 4000 at 2 $A.g^{-1}$	[104]
	$Zn(CF_3SO_3)_2$ PAM Hydrogel		8.2 $\mu Wh.cm^{-2}$	40 $\mu W.cm^{-2}$	95 after 100 at 1 $mA.cm^{-2}$	
Zn//Mesoporous Carbon	1 M $Zn(CF_3SO_3)_2$ in acetonitrile	0–1.8	92.7	179	~100 after 10000 at 2 $A.g^{-1}$	[105]
Zn//Mesoporous AC	2 M $ZnSO_4$	0.3–1.8	188	533	93 after 1500 at 0.5 $A.g^{-1}$	[106]
Zn//Oxidized CNTs	1 M $ZnSO_4$, $ZnSO_4$–PVA gel	0–1.8	–	–	~100 after 5 times (5 cyc at 5 $mV.s^{-1}$ and 1000 cycles at 5 $mV.s^{-1}$)	[107]
Zn/porous carbon//porous carbon	3 M $Zn(ClO_4)_2$	0–1.9	104.8	58	99.2 after 30000 at 20 $A.g^{-1}$	[95]
Zn@carbon cloth//oxygen rich porous carbon	Gelatin/$ZnSO_4$ gel	0.2–1.8	82.36	44.14	87.6 after 10000 at 1 $A.g^{-1}$	[108]
Zn//P&B doped AC	2 M $ZnSO_4$	0.3–1.9	169.4	500	95 after 2000 at 0.5 $A.g^{-1}$	[109]
Z-n//PA–COF	1 M Z–nSO_4	0.2–1.6	–	–	0.38 per cycle within 10000 at 1 $A.g^{-1}$	[110]
Zn//Phosphorene	WIS (21 M LiTFSI + 1 M $Zn(CF_3SO_3)_2$)	0.8–2.2	204.4	18787.7	~100 after 5000 at 0.5 $A.g^{-1}$	[111]
	0.2 M $ZnCl_2$ in Et_4NBF_4/PC	0.8–2.2	315.6	23582.4	~64 after 9500 at 0.5 $A.g^{-1}$	
Zn//bio-waste derived carbon	1 M $Zn(CF_3SO_3)_2$	0.2–1.8	147.0	136.1	92.2 after 10000 at 10 $A.g^{-1}$	[112]
Zn//$RuO_2 \cdot H_2O$	2 M $Zn(CF_3SO_3)_2$	0.4–1.6	82	16740	87.5 after 10000 at 20 $A.g^{-1}$	[113]
Zn//S doped porous carbon	2 M $ZnSO_4$	0.2–1.8	162.6	160	96.8 after 18000 at 20 $A.g^{-1}$	[114]
Zn@Ti_3C_2//Ti_3C_2	Gelatin-1 M $ZnSO_4$ gel	0.1–1.35	–	–	82.5 after 1000 at 3 $A.g^{-1}$	[115]
Zn//Silk derived AC	Zn ion containing PAM hydrogel	0.2–1.8	217	450	95.1 after 100000	[116]
Zn//TiN	1 M $ZnSO_4$	0.1–1.9	135	186	64.2 after 10000 at 1 $A.g^{-1}$	[117]
Zn//AC	SA–Zn–Br hydrogel	0–2.6	605	1848	87.7 after 5000 at 6 $A.g^{-1}$	[118]
Zn//reduced graphene hydrogel	1 M $ZnSO_4$	0.2–1.6	100.9	70	92.06 after 10000 at 5 $A.g^{-1}$	[119]

clusters are lower than that of their corresponding $[Zn(H_2O)_n]^{2+}$ counterparts. Therefore, these clusters are easily desolvated during the charging-discharging process of the ZIC, acquiring a large surface area and thereby the high storage capacity. In another study, Huang et al.[121] studied the influence of the type of anions of electrolyte on the capacitive and anti-self-discharging capability of the TiN cathode. Three different anions were considered by using the electrolytic salts of $ZnSO_4$, $ZnAc_2$ and $ZnCl_2$. Adsorption energies and adsorption positions of different anions on TiN material were calculated using DFT, suggesting SO_4^- ions have the lowest adsorption energy and excellent electrochemical performance. The ZIC showed excellent anti-self-discharging capability with huge capacitance retention of 83.92% after 500 h resting time. This work paves the way for trying different electrolytes and investigating the interfaces at the electrode/electrolyte.

In another work, to improve the energy density, Han et al.[122] prepared redox additive bromide ion hydrogel electrolyte (SA–Zn–Br) for flexible ZIC. The details of the preparation of hydrogel electrolyte and the charge storage mechanism of the ZIC are shown in Figure 8. This redox additive introduces additional faradaic reactions and thereby enhances the energy density of the cell. The flexible ZIC was fabricated using AC cathode, Zn foil anode and the redox additive-based hydrogel electrolyte. This ZIC demonstrated a maximum energy density of 605 $Wh \cdot kg^{-1}$ at a power density of 1848 $W \cdot kg^{-1}$ in a voltage range of 2.6 V. The cyclic stability of the ZIC was found to be 87.7% after 5000 GCD cycles.

Apart from this, the water decomposition at a certain potential is a limiting factor of utilizing aqueous electrolytes for ZICs. The operating potential window of the aqueous electrolyte can be widened by preparing a WiS electrolyte. The concept of WiS electrolyte was proposed by Wang et al.,[123] they successfully widened the potential window up to 3 V. The WiS is nothing but preparing an electrolyte with ultrahigh concentration, in which, the decomposition of water is inhibited owing to the close interaction of water molecules with electrolytic ions. Huang et al.,[101] recently used the WiS electrolyte for phosphorene-based ZIC that expanded a potential window up to 2.2 V and delivered a specific capacitance of 214.3 $F \cdot g^{-1}$ after 5000 cycles. In the same work, the ZIC fabricated with non-aqueous electrolyte (Et_4NBF_4/PC) operates in a potential window of 2.5 V, demonstrating a specific capacitance of 105.9 $F \cdot g^{-1}$ even after 9500 cycles. Therefore, most of the efforts were made to improve the energy density of the cell by using electrolytes with different salts, adding redox additives, utilizing WiS electrolytes, etc.

In summary, several anode, cathode and electrolyte materials have been reported for ZIC in literature. Each of these materials has its advantages and disadvantages which are summarized in Table 4. In addition, as shown in Figure 9a, the energy and power densities (Ragone plot) of reported ZICs have been plotted along with other energy storage systems includ-

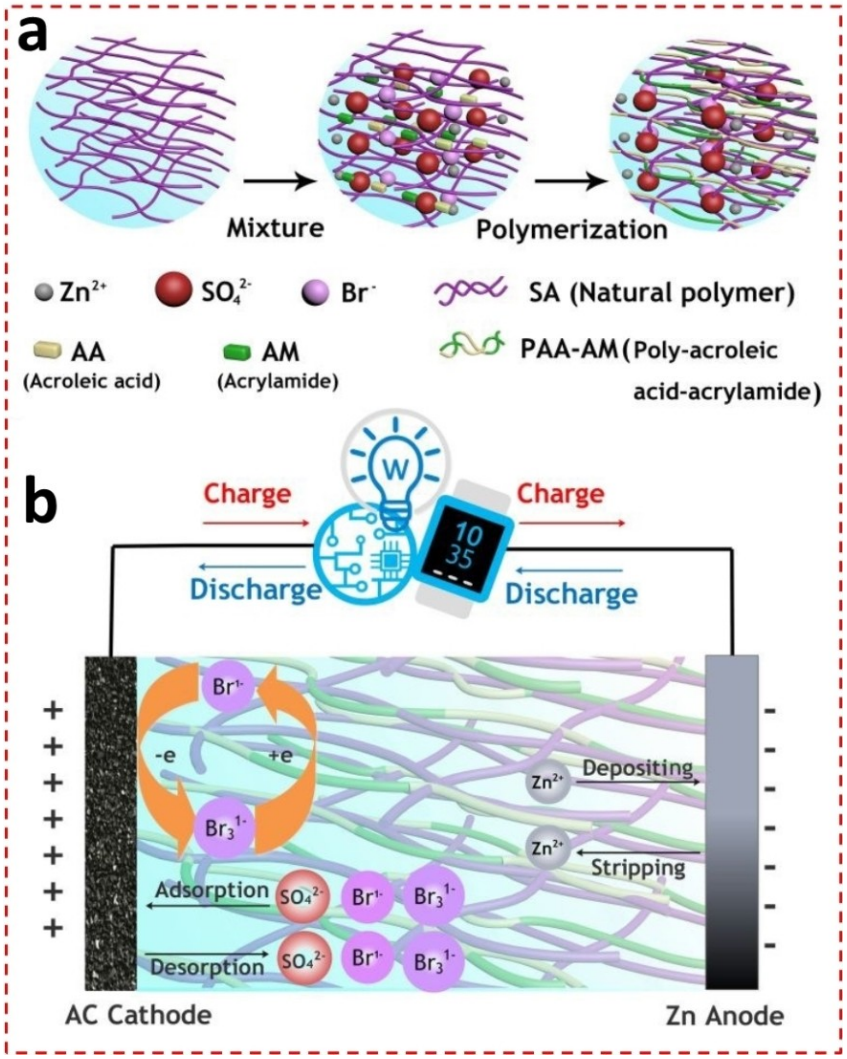

Figure 8. (a) Schematic preparation of bromide ion hydrogel electrolyte (b) Charge storage mechanism of ZIC based on bromide ion hydrogel electrolyte, (a–b) reproduced with permission from the ref. [122]. Copyright 2020, Royal Society of Chemistry.

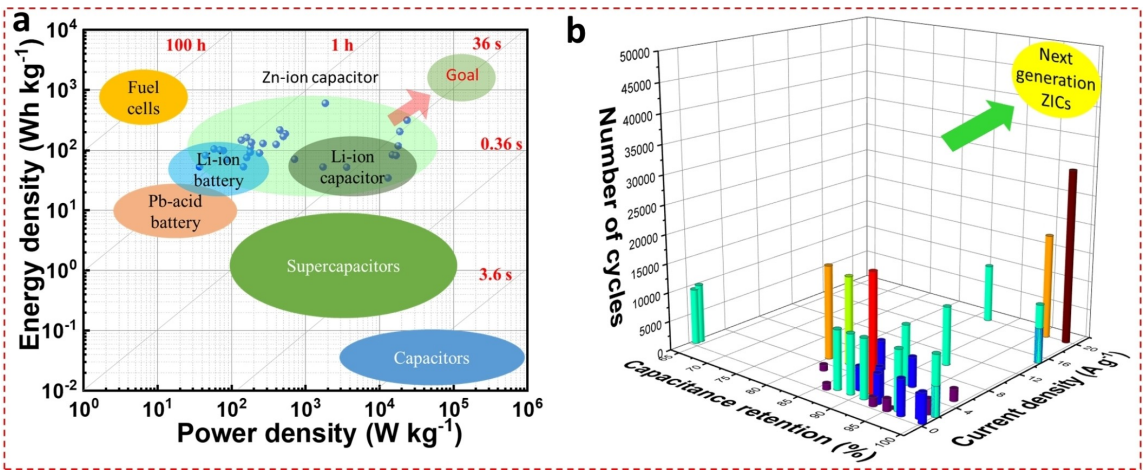

Figure 9. (a) Ragone plot and (b) cyclic stability performance of ZICs reported so far.

Table 4. Advantages and disadvantages of materials used in ZICs.

Type	Material	Advantages	Disadvantages
Anode	Zn foil	High theoretical capacity (820 mAh·g^{-1}), non-toxic, inexpensive, abundant, and safe.	Presence of dendrite formation and side reactions and instability in aqueous electrolytes, etc.
	TiS_2	Large interlayer spacing (5.7 Å), low insertion potential (0.3 V vs Zn^{2+}/Zn) and absence of dendrite formation and byproducts.	Relatively lower specific capacity and structural changes during insertion/extraction lead to poor cyclic performance.
	AC	Inexpensive and abundance	Formation of byproducts
	Porous carbon	Low cost, abundance, sustainable and high surface area	Poor ionic diffusion and transport abilities, inferior wettability and electrical conductivity
	Graphene	High theoretical specific surface area (~2,600 m^2·g), good electronic conductivity and excellent mechanical strength.	Irreversible restacking of sheets
Cathode	MXenes	High conductivity and good hydrophilicity	Inadequate interlayer spacing and spontaneous restacking of nanosheets
	Phosphorene	High specific surface area, good electrical conductivity (300 S·m^{-1}), huge channel size (3.08 Å) and rapid ion diffusion.	Unscalable production, intricate synthesis procedure, instability of few-layer phosphorene and poor storage performance
	RuO_2	Good electrical conductivity and high theoretical specific capacitance	High cost, toxicity and scarcity
Electrolyte	Aqueous	High safety, low cost, abundance eco-friendliness, and excellent compatibility with the electrodes	The presence of free water leads to H_2 generation on Zn anode and a low potential window (~1.23 V)
	Non-aqueous	A wide potential window (~3.8 V vs. Zn^{2+}/Zn), avoids water-induced side reactions, stabilizes zinc anodes and enhances coulombic efficiency.	Poor ionic conductivity and desolation kinetics, flammable and volatile

ing SCs, batteries and hybrid SCs. There is much scope in improving the energy and power densities of ZICs for advanced applications such as hybrid electric vehicles and plug-in hybrid electric vehicles as indicated in the Ragone plot. Additionally, since the hybrid ZICs are mainly hindered by their poor cyclic stability, much work is anticipated to enhance cyclability and develop next-generation ZICs (Figure 9b).

4. Summary and future prospects

In this review, we presented recent developments in the anode and cathode materials of ZIC. Different aspects including the design, construction and working of SCs, ZIB and ZIC have been discussed along with their charge storage mechanisms. The electrode material engineering, device configuration, energy storage mechanism and electrochemical performance of ZIC have been summarized. The development of ZIC can be discussed as follows,

1. It has been demonstrated that different anode materials have been developed for ZIC including surface-modified Zn, TiS_2, AC, etc.
2. The dendrite formation and side reactions on the Zn anode have been effectively suppressed by coating corrosion inhibitors on the anode and by introducing an artificial layer in between the anode and separator. Besides, the diffusion pathways have been reduced by roughening and creating nanoarchitectures on the Zn anode.
3. In the development of cathode materials, different efforts have been made to improve the capacitive performance of cathode materials including the enhancement of porosity and wettability of carbon, heteroatom doping, incorporation of redox materials and introduction of advanced materials including MXenes, Phosphorene, etc.
4. In addition, advanced strategies have been implemented including the introduction of mesopores and macropores, construction of hollow bowl-like carbon and enhancement of interlayer spacing with controlled restacking of 2D nanosheets.
5. Different electrolytes have been devolved such as aqueous, nonaqueous and water in salt for ZIC with enhanced storage performance.

Besides these accomplishments, there is still much opportunity for the further development of high-performance ZICs. The potential future research directions and the challenges are summarized as follows,

1. The different novel anode and cathode materials with high capacity and cyclic stability should be developed. It is highly desirable to deconvolute capacitive and diffusion-controlled contributions of capacity in both anode and cathode materials. Anode materials with high capacitive contribution are recommended to combine with capacitive cathode to match the rate capabilities of both anode and cathode.
2. The major issues of Zn metal anode are the formation of dendrites, low columbic efficiency, and corrosion. These issues can be rectified by developing nanostructured and high surface area Zn-based anode materials.
3. The dendrite formation of Zn can be inhibited by modifying the interfacial properties of Zn-based anodes such as exposing coatings with facets of least Zn affinity.
4. Since very few electrolytes have been studied for ZIC, much research is recommended for developing novel electrolytes to suppress the electrolysis of water and to enhance the operating potential and thereby the energy density of the ZIC. The preparation and characterization of hydrogels and water-in-salt electrolytes can be a promising direction.
5. The aqueous electrolytes are mostly preferred because of their environmental friendliness, low cost and excellent ionic conductivity. However, the hydrogen evolution and the

lower potential window limit their promising application. These issues can be addressed by developing novel additives that may offer high electrochemical stability. Additionally, the development of non-aqueous electrolytes can be considered.

6. The dominant reaction on the cathode is the physical adsorption/desorption of electrolyte ions. It is highly recommended to develop a high surface area cathode with meso, micro and macropore size distribution. The major issue with carbon-based cathode materials is their poor capacity that can be addressed by researching novel pseudocapacitive cathodes such as MXenes and phosphorene. It is desirable to develop a cathode with a high capacity and multi-dimensional hierarchical structure.
7. There is a high demand for flexible energy storage devices for next-generation wearable electronics. The flexible ZIC can be a low-cost and environmentally friendly storage solution. Therefore, much research is expected to develop high-performance flexible ZIC. Novel flexible components such as anodes, cathodes and electrolytes should be developed.

Acknowledgements

ADJ is thankful to the Department of Science and Technology (DST), Govt. of India for financial assistance under the DST INSPIRE Faculty Scheme [DST/INSPIRE/04/2017/002737].

Conflict of Interest

The authors declare no conflict of interest.

Keywords: anode · cathode · hybrid zinc ion capacitor · supercapacitor · zinc ion battery

[1] F. Martins, C. Felgueiras, M. Smitková, *Energy Procedia* **2018**, *153*, 107–111.
[2] J. Benedek, T.-T. Sebestyén, B. Bartók, *Renewable Sustainable Energy Rev.* **2018**, *90*, 516–535.
[3] S. R. Sinsel, R. L. Riemke, V. H. Hoffmann, *Renewable Energy* **2020**, *145*, 2271–2285.
[4] J. Liu, J. Wang, C. Xu, H. Jiang, C. Li, L. Zhang, J. Lin, Z. X. Shen, *Adv. Sci.* **2018**, *5*, 1700322.
[5] P. Zhang, F. Wang, M. Yu, X. Zhuang, X. Feng, *Chem. Soc. Rev.* **2018**, *47*, 7426–7451.
[6] D. P. Dubal, O. Ayyad, V. Ruiz, P. Gómez-Romero, *Chem. Soc. Rev.* **2015**, *44*, 1777–1790.
[7] G. Nagaraju, S. C. Sekhar, B. Ramulu, J. S. Yu, *Small* **2019**, *15*, 1805418.
[8] L. Kouchachvili, W. Yaïci, E. Entchev, *J. Power Sources* **2018**, *374*, 237–248.
[9] D. P. Dubal, J. G. Kim, Y. Kim, R. Holze, C. D. Lokhande, W. B. Kim, *Energy Technol.* **2014**, *2*, 325–341.
[10] A. Jagadale, X. Zhou, R. Xiong, D. P. Dubal, J. Xu, S. Yang, *Energy Storage Mater.* **2019**, *19*, 314–329.
[11] J. Yin, W. Zhang, N. A. Alhebshi, N. Salah, H. N. Alshareef, *Small Methods* **2020**, *4*, 1900853.
[12] D.-G. Wang, Z. Liang, S. Gao, C. Qu, R. Zou, *Coord. Chem. Rev.* **2020**, *404*, 213093.
[13] B. Xu, H. Zhang, H. Mei, D. Sun, *Coord. Chem. Rev.* **2020**, *420*, 213438.
[14] Y. Wang, Y. Song, Y. Xia, *Chem. Soc. Rev.* **2016**, *45*, 5925–5950.
[15] M. Z. Iqbal, M. M. Faisal, S. R. Ali, *Int. J. Energy Res.* **2021**, *45*, 1449–1479.
[16] S. Wu, F. Zhang, Y. Tang, *Adv. Sci.* **2018**, *5*, 1701082.
[17] G. Zhang, X. Ou, C. Cui, J. Ma, J. Yang, Y. Tang, *Adv. Funct. Mater.* **2019**, *29*, 1806722.
[18] X. Zhang, Y. Tang, F. Zhang, C.-S. Lee, *Adv. Energy Mater.* **2016**, *6*, 1502588.
[19] F. Wang, X. Wu, X. Yuan, Z. Liu, Y. Zhang, L. Fu, Y. Zhu, Q. Zhou, Y. Wu, W. Huang, *Chem. Soc. Rev.* **2017**, *46*, 6816–6854.
[20] C. Zhong, Y. Deng, W. Hu, J. Qiao, L. Zhang, J. Zhang, *Chem. Soc. Rev.* **2015**, *44*, 7484–7539.
[21] M. R. Lukatskaya, B. Dunn, Y. Gogotsi, *Nat. Commun.* **2016**, *7*, 12647.
[22] A. Muzaffar, M. B. Ahamed, K. Deshmukh, J. Thirumalai, *Renewable Sustainable Energy Rev.* **2019**, *101*, 123–145.
[23] R. Bi, N. Xu, H. Ren, N. Yang, Y. Sun, A. Cao, R. Yu, D. Wanc, *Angew. Chem. Int. Ed.* **2020**, *59*, 4865–4868; *Angew. Chem.* **2020**, *132*, 4895–4898.
[24] P. Cai, K. Zou, G. Zou, H. Hou, X. Ji, *Nanoscale* **2020**, *12*, 3677–3685.
[25] Y.-K. Wang, M.-C. Liu, J. Cao, H.-J. Zhang, L.-B. Kong, D. P. Trudgeon, X. Li, F. C. Walsh, *ACS Appl. Mater. Interfaces* **2020**, *12*, 3709–3718.
[26] C. Sun, X. Zhang, C. Li, K. Wang, X. Sun, Y. Ma, *Energy Storage Mater.* **2020**, *24*, 160–166.
[27] Z. Le, F. Liu, P. Nie, X. Li, X. Liu, Z. Bian, G. Chen, H. B. Wu, Y. Lu, *ACS Nano* **2017**, *11*, 2952–2960.
[28] Z. Chen, V. Augustyn, X. Jia, Q. Xiao, B. Dunn, Y. Lu, *ACS Nano* **2012**, *6*, 4319–4327.
[29] J. Ding, H. Wang, Z. Li, K. Cui, D. Karpuzov, X. Tan, A. Kohandehghan, D. Mitlin, *Energy Environ. Sci.* **2015**, *8*, 941–955.
[30] X. Wang, S. Kajiyama, H. Iinuma, E. Hosono, S. Oro, I. Moriguchi, M. Okubo, A. Yamada, *Nat. Commun.* **2015**, *6*, 6544.
[31] S. Komaba, T. Hasegawa, M. Dahbi, K. Kubota, *Electrochem. Commun.* **2015**, *60*, 172–175.
[32] J. Chen, B. Yang, H. Hou, H. Li, L. Liu, L. Zhang, X. Yan, *Adv. Energy Mater.* **2019**, *9*, 1803894.
[33] S. Dong, Z. Li, Z. Xing, X. Wu, X. Ji, X. Zhang, *ACS Appl. Mater. Interfaces* **2018**, *10*, 15542–15547.
[34] Z. Zhang, M. Li, Y. Gao, Z. Wei, M. Zhang, C. Wang, Y. Zeng, B. Zou, G. Chen, F. Du, *Adv. Funct. Mater.* **2018**, *28*, 1802684.
[35] H. Wang, W. Ye, Y. Yang, Y. Zhong, Y. Hu, *Nano Energy* **2021**, *85*, 105942.
[36] H. Zhang, K. Ye, K. Zhu, R. Cang, X. Wang, G. Wang, D. Cao, *ACS Sustainable Chem. Eng.* **2017**, *5*, 6727–6735.
[37] X. Cao, L. Wang, J. Chen, J. Zheng, *ChemElectroChem* **2018**, *5*, 2789–2794.
[38] Z. Tian, X. Tong, G. Sheng, Y. Shao, L. Yu, V. Tung, J. Sun, R. B. Kaner, Z. Liu, *Nat. Commun.* **2019**, *10*, 4913.
[39] H. Zhang, D. Cao, X. Bai, H. Xie, X. Liu, X. Jiang, H. Lin, H. He, *ACS Sustainable Chem. Eng.* **2019**, *7*, 6113–6121.
[40] N. Wu, W. Yao, X. Song, G. Zhang, B. Chen, J. Yang, Y. Tang, *Adv. Energy Mater.* **2019**, *9*, 1803865.
[41] Z. Li, K. Xiang, W. Xing, W. C. Carter, Y.-M. Chiang, *Adv. Energy Mater.* **2015**, *5*, 1401410.
[42] F. Wang, Z. Liu, X. Wang, X. Yuan, X. Wu, Y. Zhu, L. Fu, Y. Wu, *J. Mater. Chem. A* **2016**, *4*, 5115–5123.
[43] K. Li, Y. Shao, S. Liu, Q. Zhang, H. Wang, Y. Li, R. B. Kaner, *Small* **2017**, *13*, 1700380.
[44] J. Shi, S. Wang, Q. Wang, X. Chen, X. Du, M. Wang, Y. Zhao, C. Dong, L. Ruan, W. Zeng, *J. Power Sources* **2020**, *446*, 227345.
[45] Y. Zheng, W. Zhao, D. Jia, Y. Liu, L. Cui, D. Wei, R. Zheng, J. Liu, *Chem. Eng. J.* **2020**, *387*, 124161.
[46] B. D. Boruah, A. Mathieson, B. Wen, C. Jo, F. Deschler, M. De Volder, *Nano Lett.* **2020**, *20*, 5967–5974.
[47] M. Liu, L. Chang, Z. Le, J. Jiang, J. Li, H. Wang, C. Zhao, T. Xu, P. Nie, L. Wang, *ChemSusChem* **2020**, *13*, 5837–5862.
[48] H. Wang, C. Zhu, D. Chao, Q. Yan, H. J. Fan, *Adv. Mater.* **2017**, *29*, 1702093.
[49] Y. Tian, R. Amal, D.-W. Wang, *Front. Energy Res.* **2016**, *4*, DOI 10.3389/fenrg.2016.00034.
[50] J. Ming, J. Guo, C. Xia, W. Wang, H. N. Alshareef, *Mater. Sci. Eng. R. Rep.* **2019**, *135*, 58–84.
[51] B. Tang, L. Shan, S. Liang, J. Zhou, *Energy Environ. Sci.* **2019**, *12*, 3288–3304.
[52] H. Li, L. Ma, C. Han, Z. Wang, Z. Liu, Z. Tang, C. Zhi, *Nano Energy* **2019**, *62*, 550–587.

[53] A. Konarov, N. Voronina, J. H. Jo, Z. Bakenov, Y.-K. Sun, S.-T. Myung, *ACS Energy Lett.* **2018**, *3*, 2620–2640.
[54] M. Song, H. Tan, D. Chao, H. J. Fan, *Adv. Funct. Mater.* **2018**, *28*, 1802564.
[55] G. Fang, J. Zhou, A. Pan, S. Liang, *ACS Energy Lett.* **2018**, *3*, 2480–2501.
[56] L. Dong, W. Yang, W. Yang, Y. Li, W. Wu, G. Wang, *J. Mater. Chem. A* **2019**, *7*, 13810–13832.
[57] H. Tang, J. Yao, Y. Zhu, *Adv. Energy Mater.* **2021**, *11*, 2003994.
[58] Q. Liu, H. Zhang, J. Xie, X. Liu, X. Lu, *Carbon Energy* **2020**, *2*, 521–539.
[59] Y. Shao, F. Shen, Y. Shao, *ChemElectroChem* **2021**, *8*, 484–491.
[60] Z. Li, Y. An, S. Dong, C. Chen, L. Wu, Y. Sun, X. Zhang, *Energy Storage Mater.* **2020**, *31*, 252–266.
[61] M. Yousaf, H. T. H. Shi, Y. Wang, Y. Chen, Z. Ma, A. Cao, H. E. Naguib, R. P. S. Han, *Adv. Energy Mater.* **2016**, *6*, 1600490.
[62] A. Davies, A. Yu, *Can. J. Chem. Eng.* **2011**, *89*, 1342–1357.
[63] V. Augustyn, P. Simon, B. Dunn, *Energy Environ. Sci.* **2014**, *7*, 1597–1614.
[64] D. Chen, M. Lu, D. Cai, H. Yang, W. Han, *J. Energy Chem.* **2021**, *54*, 712–726.
[65] H. Wang, M. Wang, Y. Tang, *Energy Storage Mater.* **2018**, *13*, 1–7.
[66] L. Dong, X. Ma, Y. Li, L. Zhao, W. Liu, J. Cheng, C. Xu, B. Li, Q.-H. Yang, F. Kang, *Energy Storage Mater.* **2018**, *13*, 96–102.
[67] D. Han, S. Wu, S. Zhang, Y. Deng, C. Cui, L. Zhang, Y. Long, H. Li, Y. Tao, Z. Weng, Q.-H. Yang, F. Kang, *Small* **2020**, *16*, 2001736.
[68] Q. Zhang, J. Luan, X. Huang, Q. Wang, D. Sun, Y. Tang, X. Ji, H. Wang, *Nat. Commun.* **2020**, *11*, 3961.
[69] Z. Li, W. Deng, C. Li, W. Wang, Z. Zhou, Y. Li, X. Yuan, J. Hu, M. Zhang, J. Zhu, W. Tang, X. Wang, R. Li, *J. Mater. Chem. A* **2020**, *8*, 17725–17731.
[70] L. Dong, W. Yang, W. Yang, H. Tian, Y. Huang, X. Wang, C. Xu, C. Wang, F. Kang, G. Wang, *Chem. Eng. J.* **2020**, *384*, 123355.
[71] G.-H. An, J. Hong, S. Pak, Y. Cho, S. Lee, B. Hou, S. Cha, *Adv. Energy Mater.* **2020**, *10*, 1902981.
[72] G.-H. An, S. Cha, J. I. Sohn, *Appl. Surf. Sci.* **2019**, *467–468*, 1157–1160.
[73] G. An, *Curr. Appl. Phys.* **2020**, *20*, 605–610.
[74] P. Liu, W. Liu, Y. Huang, P. Li, J. Yan, K. Liu, *Energy Storage Mater.* **2020**, *25*, 858–865.
[75] Q. Wang, S. Wang, J. Li, L. Ruan, N. Wei, L. Huang, Z. Dong, Q. Cheng, Y. Xiong, W. Zeng, *Adv. Electron. Mater.* **2020**, *6*, 2000388.
[76] X. Ma, J. Cheng, L. Dong, W. Liu, J. Mou, L. Zhao, J. Wang, D. Ren, J. Wu, C. Xu, F. Kang, *Energy Storage Mater.* **2019**, *20*, 335–342.
[77] X. Ma, J. Wang, X. Wang, L. Zhao, C. Xu, *J. Mater. Sci. Mater. Electron.* **2019**, *30*, 5478–5486.
[78] B. D. Boruah, B. Wen, S. Nagane, X. Zhang, S. D. Stranks, A. Boies, M. De Volder, *ACS Energy Lett.* **2020**, *5*, 3132–3139.
[79] Z. Jian, N. Yang, M. Vogel, S. Leith, A. Schulte, H. Schönherr, T. Jiao, W. Zhang, J. Müller, B. Butz, X. Jiang, *Adv. Energy Mater.* **2020**, *10*, 2002202.
[80] S. Chen, G. Yang, X. Zhao, N. Wang, T. Luo, X. Chen, T. Wu, S. Jiang, P. A. van Aken, S. Qu, T. Li, L. Du, J. Zhang, H. Wang, H. Wang, *Front. Chem.* **2020**, *8*, 663.
[81] T. Ni, S. Wang, J. Shi, X. Du, Q. Cheng, Z. Dong, L. Ruan, W. Zeng, X. Guo, X. Ren, Z. Huang, *Adv. Mater.* **2020**, *5*, 2000268.
[82] J. Shi, S. Wang, Q. Wang, X. Chen, X. Du, M. Wang, Y. Zhao, C. Dong, L. Ruan, W. Zeng, *J. Power Sources* **2020**, *446*, 227345.
[83] S. Wang, Q. Wang, W. Zeng, M. Wang, L. Ruan, Y. Ma, *Nano-Micro Lett.* **2019**, *11*, 70.
[84] L. Dong, X. Ma, Y. Li, L. Zhao, W. Liu, J. Cheng, C. Xu, B. Li, Q.-H. Yang, F. Kang, *Energy Storage Mater.* **2018**, *13*, 96–102.
[85] H. Wang, M. Wang, Y. Tang, *Energy Storage Mater.* **2018**, *13*, 1–7.
[86] Z. Liu, G. Li, T. Cui, A. Borodin, C. Kuhl, F. Endres, *J. Solid State Electrochem.* **2018**, *22*, 91–101.
[87] C. Li, Z. Sun, T. Yang, L. Yu, N. Wei, Z. Tian, J. Cai, J. Lv, Y. Shao, M. H. Rümmeli, J. Sun, Z. Liu, *Adv. Mater.* **2020**, *32*, 2003425.
[88] G.-H. An, *Appl. Surf. Sci.* **2020**, *530*, 147220.
[89] Y.-G. Lee, G.-H. An, *ACS Appl. Mater. Interfaces* **2020**, *12*, 41342–41349.
[90] D. Wang, S. Wang, Z. Lu, *Int. J. Energy Res.* **2021**, *45*, 2498–2510.
[91] R. Fei, H. Wang, Q. Wang, R. Qiu, S. Tang, R. Wang, B. He, Y. Gong, H. J. Fan, *Adv. Energy Mater.* **2020**, 10, 2002741.
[92] C. Jiang, Z. Zou, *Diamond Relat. Mater.* **2020**, *101*, 107603.
[93] J. Zeng, L. Dong, L. Sun, W. Wang, Y. Zhou, L. Wei, X. Guo, *Nano-Micro Lett.* **2020**, *13*, 19.
[94] Z. Li, D. Chen, Y. An, C. Chen, L. Wu, Z. Chen, Y. Sun, X. Zhang, *Energy Storage Mater.* **2020**, *28*, 307–314.
[95] J. Yin, W. Zhang, W. Wang, N. A. Alhebshi, N. Salah, H. N. Alshareef, *Adv. Energy Mater.* **2020**, *10*, 2001705.
[96] Y. Zhu, X. Ye, H. Jiang, J. Xia, Z. Yue, L. Wang, Z. Wan, C. Jia, X. Yao, *J. Power Sources* **2020**, *453*, 227851.
[97] T. Ni, S. Wang, J. Shi, X. Du, Q. Cheng, Z. Dong, L. Ruan, W. Zeng, X. Guo, X. Ren, Z. Huang, *Adv. Mater.* **2020**, *5*, 2000268.
[98] X. Li, M. Li, Q. Yang, D. Wang, L. Ma, G. Liang, Z. Huang, B. Dong, Q. Huang, C. Zhi, *Adv. Energy Mater.* **2020**, *10*, 2001394.
[99] Q. Wang, S. Wang, X. Guo, L. Ruan, N. Wei, Y. Ma, J. Li, M. Wang, W. Li, W. Zeng, *Adv. Electron. Mater.* **2019**, *5*, 1900537.
[100] Q. Yang, Z. Huang, X. Li, Z. Liu, H. Li, G. Liang, D. Wang, Q. Huang, S. Zhang, S. Chen, C. Zhi, *ACS Nano* **2019**, *13*, 8275–8283.
[101] Z. Huang, A. Chen, F. Mo, G. Liang, X. Li, Q. Yang, Y. Guo, Z. Chen, Q. Li, B. Dong, C. Zhi, *Adv. Energy Mater.* **2020**, *10*, 2001024.
[102] L. Dong, W. Yang, W. Yang, C. Wang, Y. Li, C. Xu, S. Wan, F. He, F. Kang, G. Wang, *Nano-Micro Lett.* **2019**, *11*, 94.
[103] B. D. Boruah, A. Mathieson, B. Wen, C. Jo, F. Deschler, M. De Volder, *Nano Lett.* **2020**, *20*, 5967–5974.
[104] J. Zeng, L. Dong, L. Sun, W. Wang, Y. Zhou, L. Wei, X. Guo, *Nano-Micro Lett.* **2020**, *13*, 19.
[105] C. Jiang, Z. Zou, *Diamond Relat. Mater.* **2020**, *101*, 107603.
[106] G.-H. An, *Appl. Surf. Sci.* **2020**, *530*, 147220.
[107] Y. Tian, R. Amal, D.-W. Wang, *Front. Energy Res.* **2016**, *4*, 34.
[108] Y. Zheng, W. Zhao, D. Jia, Y. Liu, L. Cui, D. Wei, R. Zheng, J. Liu, *Chem. Eng. J.* **2020**, *387*, 124161.
[109] Y.-G. Lee, G.-H. An, *ACS Appl. Mater. Interfaces* **2020**, *12*, 41342–41349.
[110] W. Wang, V. S. Kale, Z. Cao, S. Kandambeth, W. Zhang, J. Ming, P. T. Parvatkar, E. Abou-Hamad, O. Shekhah, L. Cavallo, M. Eddaoudi, H. N. Alshareef, *ACS Energy Lett.* **2020**, *5*, 2256–2264.
[111] Z. Huang, A. Chen, F. Mo, G. Liang, X. Li, Q. Yang, Y. Guo, Z. Chen, Q. Li, B. Dong, C. Zhi, *Adv. Energy Mater.* **2020**, *10*, 2001024.
[112] Z. Li, D. Chen, Y. An, C. Chen, L. Wu, Z. Chen, Y. Sun, X. Zhang, *Energy Storage Mater.* **2020**, *28*, 307–314.
[113] L. Dong, W. Yang, W. Yang, C. Wang, Y. Li, C. Xu, S. Wan, F. He, F. Kang, G. Wang, *Nano-Micro Lett.* **2019**, *11*, 94.
[114] D. Wang, S. Wang, Z. Lu, *Int. J. Energy Res.* **2021**, *45*, 2498–2510.
[115] Q. Yang, Z. Huang, X. Li, Z. Liu, H. Li, G. Liang, D. Wang, Q. Huang, S. Zhang, S. Chen, C. Zhi, *ACS Nano* **2019**, *13*, 8275–8283.
[116] C. Wang, Z. Pei, Q. Meng, C. Zhang, X. Sui, Z. Yuan, S. Wang, Y. Chen, *Angew. Chem. Int. Ed.* **2021**, *60*, 990–997; *Angew. Chem.* **2021**, *133*, 1003–1010.
[117] Z. Huang, T. Wang, H. Song, X. Li, G. Liang, D. Wang, Q. Yang, Z. Chen, L. Ma, Z. Liu, B. Gao, J. Fan, C. Zhi, *Angew. Chem. Int. Ed.* **2021**, *60*, 1011–1021; *Angew. Chem.* **2021**, *133*, 1024–1034.
[118] L. Han, H. Huang, J. Li, X. Zhang, Z. Yang, M. Xu, L. Pan, *J. Mater. Chem. A* **2020**, *8*, 15042–15050.
[119] G. Sun, Y. Xiao, B. Lu, X. Jin, H. Yang, C. Dai, X. Zhang, Y. Zhao, L. Qu, *ACS Appl. Mater. Interfaces* **2020**, *12*, 7239–7248.
[120] C. Wang, Z. Pei, Q. Meng, C. Zhang, X. Sui, Z. Yuan, S. Wang, Y. Chen, *Angew. Chem. Int. Ed.* **2021**, *60*, 990–997; *Angew. Chem.* **2021**, *133*, 1003–1010.
[121] Z. Huang, T. Wang, H. Song, X. Li, G. Liang, D. Wang, Q. Yang, Z. Chen, L. Ma, Z. Liu, B. Gao, J. Fan, C. Zhi, *Angew. Chem. Int. Ed.* **2021**, *60*, 1011–1021; *Angew. Chem.* **2021**, *133*, 1024–1034.
[122] L. Han, H. Huang, J. Li, X. Zhang, Z. Yang, M. Xu, L. Pan, *J. Mater. Chem. A* **2020**, *8*, 15042–15050.
[123] L. Suo, O. Borodin, T. Gao, M. Olguin, J. Ho, X. Fan, C. Luo, C. Wang, K. Xu, *Science* **2015**, *350*, 938–943.

Manuscript received: May 26, 2021
Revised manuscript received: June 28, 2021
Accepted manuscript online: June 28, 2021
Version of record online: ■■, ■■■

MINIREVIEW

Hybrid supercapacitors have gained great research interest owing to their high energy density without the expense of power performance. Hybrid zinc ion capacitors combine the merits of zinc ion batteries and supercapacitors. This review provides recent developments in the anode, cathode and electrolyte materials of zinc ion hybrid capacitors and it describes electrode materials engineering, device configuration, energy storage mechanism and electrochemical performance.

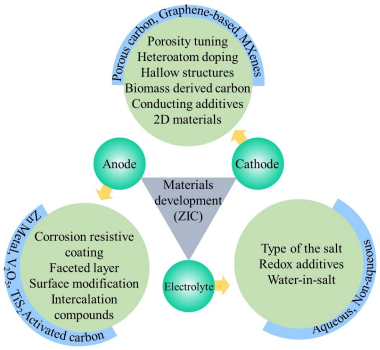

Dr. A. D. Jagadale, R. C. Rohit, Dr. S. K. Shinde, Prof. D.-Y. Kim*

1 – 18

Materials Development in Hybrid Zinc-Ion Capacitors